Thermodynamics of Solvent-Driven Water Extraction from Hypersaline Brines using Dimethyl Ether

Akshay Deshmukh[a], Zi Hao Foo[a], Caleb Stetson[b], Hyeonseok Lee[b], Christopher J. Orme[b], Aaron D. Wilson[b], John H. Lienhard[a,*]

[a] *Rohsenow Kendall Heat Transfer Laboratory, Department of Mechanical Engineering, Massachusetts Institute of Technology, 77 Massachusetts Avenue, Cambridge, MA 02139-4307, United States*
[b] *Chemical Separations Group, Idaho National Laboratory, P.O. Box 1625 MS 2208, Idaho Falls, ID 83415-2208, United States*

A. Deshmukh, Z. H. Foo, C. Stetson, H. Lee, C. J. Orme, A. D. Wilson, and J. H. Lienhard, "Thermodynamics of Solvent-Driven Water Extraction from Hypersaline Brines using Dimethyl Ether," *Chemical Engineering Journal* 434, 134391 (2022) https://doi.org/10.1016/j.cej.2021.134391

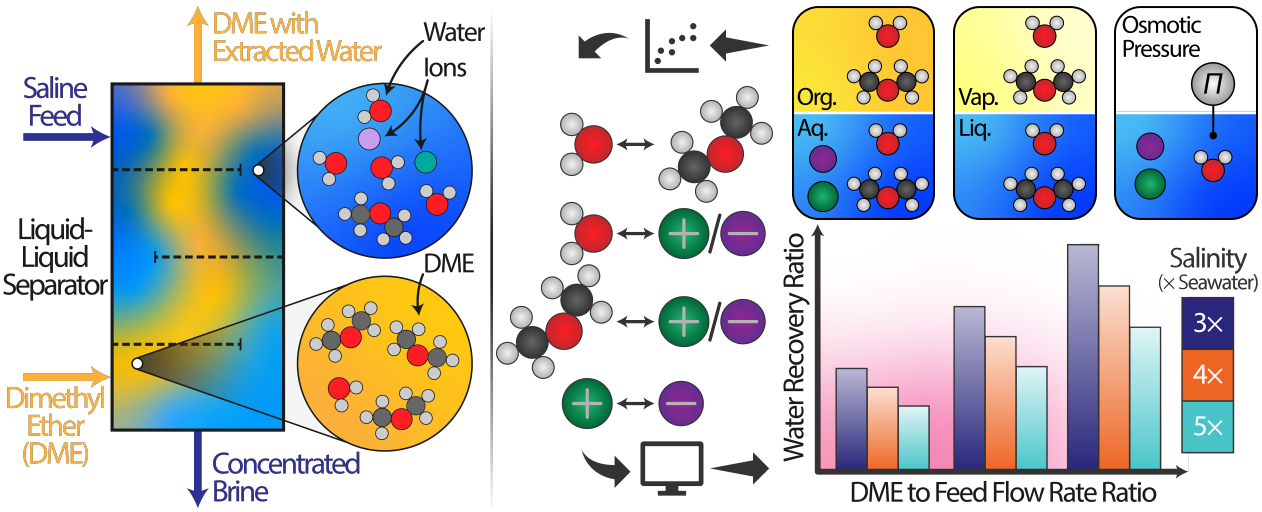

Abstract

Solvent-driven water extraction (SDWE) has promising applications in hypersaline brine desalination, including zero-liquid discharge processing for industrial wastewaters, and resource recovery, such as the extraction of lithium and rare earth elements from solution mining leachates. In this study, we develop a computational thermodynamic framework to analyze the liquid-liquid extraction of water from hypersaline brines using dimethyl ether (DME),

*Corresponding author
Email address: lienhard@mit.edu (John H. Lienhard)

an aprotic solvent that is partially miscible with water. The high volatility of DME enables its rapid separation from water–DME mixtures after water absorption, while its low polarity minimizes the organic-phase solubility of electrolytes, such as sodium chloride (NaCl). We first build a thermodynamic model based on the LIQUAC excess Gibbs free energy model for water–DME–NaCl mixtures. Maximum likelihood estimators for water–DME–NaCl interaction parameters are calculated through the nonlinear regression of fluid phase equilibrium and osmotic coefficient data using metaheuristic global optimization techniques. A multi-stage counter-current liquid-liquid separator (LLS) model is then developed to explore the water recovery and brine concentration ratios achievable as a function of feed molality and DME to feed water flow rate ratio. For a saline feed with a molality of 2.0 mol kg^{-1} (over three times the salinity of seawater) our analysis demonstrates that a one-stage LLS can achieve a water recovery ratio of 0.51 with an initial DME to saline feed molar flow rate ratio of 4.0, rising to 0.63 with a second equilibrium stage. We conclude by quantifying the amount of DME required to reach zero-liquid discharge brine salinities and analyzing the impact of staging and temperature on separation performance. Our thermodynamic model enables the rapid evaluation of SDWE systems for emerging hypersaline brine desalination and valorization applications.

Keywords: Hypersaline Desalination, Brine Concentration, Fluid Phase Equilibria, Dimethyl Ether, Zero-Liquid Discharge

1. Introduction

Desalinating hypersaline brines has the potential to recover valuable minerals from waste streams while reducing the environmental risks associated with their disposal [1, 2]. High-salinity waste streams, including mining leachate, produced water from unconventional hydrocarbon extraction, wastewater from flue gas desulfurization, landfill leachate, and concentrate from inland desalination, contain a complex mixture of salts, often including critical metals, and hazardous contaminants [3, 4]. Extracting water from these brines can simultaneously alleviate water scarcity, by increasing industrial wastewater reuse to augment freshwater supplies, and protect existing freshwater resources, by minimizing the discharge of contaminated liquid waste streams [5–7]. Furthermore, brine concentration forms an important step in the valorization of aqueous waste streams, enabling the fractional precipitation of critical materials, such as lithium, nickel, cobalt, and rare earth elements [8–16]. In addition, volume reduction through water extraction can lower the economic and environmental costs associated with transportation and storage of contaminated brines [1, 2].

Extracting water from highly-saline brines, which typically contain > 60 g kg^{-1} total dissolved solids (TDS) or > 1.0 mol kg^{-1} sodium chloride (NaCl), is inherently challenging given

their high osmotic pressure, scaling potential, and fouling propensity. Reverse osmosis (RO), the most energy-efficient desalination process, is typically restricted to retentate salinities of < 100 g kg^{-1} (< 1.7 mol kg^{-1} NaCl) to avoid exceeding the maximum operating pressures of current membranes. Furthermore, the high concentration of scale-forming ions in many industrially-relevant brines, combined with the vulnerability of membrane and heat exchanger surfaces to scaling-induced degradation, limits the use of several membrane-based and thermal desalination processes [17–20]. When treating high-salinity brines, thermal desalination systems, including multi-effect distillation (MED), multi-stage flash (MSF), and mechanical vapor compression (MVC), require extensive pretreatment and maintenance combined with corrosion-resistant materials to mitigate the deleterious impact of scaling [1, 2].

Solvent-driven water extraction (SDWE) has the potential to efficiently desalinate highly-saline feed streams up to saturation using a partially water-miscible solvent [21–32]. In SDWE, the saline feed stream is contacted with an extraction solvent, typically an organic compound, in a liquid-liquid separator (LLS) forming two distinct liquid phases. Water is extracted from the aqueous phase into the organic phase until liquid-liquid equilibrium (LLE) is reached (Figure 1). The majority of dissolved electrolytes remain in the aqueous stream, which forms the concentrated brine. The water-laden organic stream is passed to a regeneration step, where water and the extraction solvent are separated yielding purified water and recycled organic solvent. In SDWE, water-electrolyte separation occurs at a non-stationary liquid-liquid interface. Consequently, scalant precipitation and foulant deposition occur away from critical membrane or heat exchanger surfaces. Strategic selection of the extraction solvent can maximize the water recovery and salt rejection, while minimizing the energy consumption of the solvent regeneration step. Previous experimental studies have explored a range of extraction solvent chemistries, including liquid polymers [23, 24], ketones [33], nitriles [33], amines [21, 22, 30, 33, 34], and carboxylic acids [25–28, 28, 35, 36]. Solvent regeneration in each of these systems is driven by a temperature swing that lowers the water content of the organic phase at LLE.

Dimethyl ether (DME, CH_3OCH_3) is a polar aprotic organic solvent that is partially miscible with water. The low polarity of DME, which has a dielectric constant of less than 5.0, minimizes the solubility of electrolytes in the organic phase at LLE enabling near perfect salt rejection [37]. DME's high volatility—a vapor pressure of 5.9 bar at 298 K—enables the rapid and efficient separation of water–DME mixtures after extraction using energy sources ranging from electrical power to ultra-low-grade, or "waste", heat (< 50 °C) [38]. Furthermore, the low boiling point of DME, 269 K at 1.0 bar, can be leveraged to minimize fugitive solvent loss in the concentrated brine and desalinated water.

In this study, we build a computational framework to quantify the separation perfor-

mance of a SDWE system that uses DME to extract water from a highly-saline feed stream in a multistage LLS (Figure 1). We begin by developing a computational platform based on the LIQUAC excess Gibbs free energy model for aqueous-organic-electrolyte mixtures, which combines the UNIQUAC activity coefficient model for short-range interactions with a Pitzer-like electrolyte solution model for middle- and long-range interactions. Isofugacity calculations are then performed using the LIQUAC excess Gibbs free energy model combined with the Peng-Robinson Stryjek-Vera 2 (PRSV2) equation of state, to determine equilibrium phase compositions for water–DME–NaCl mixtures. LIQUAC interaction parameters are estimated through the nonlinear regression of fluid phase equilibrium and osmotic coefficient data using metaheuristic global optimization techniques. Maximum likelihood estimators for DME–Na^+ and DME–Cl^- interaction parameters are calculated for the first time using recently published liquid-liquid equilibrium (LLE) data for water–DME–NaCl mixtures. A computational model of a multistage counter-current LLS is then developed incorporating LLE calculations based on the LIQUAC excess Gibbs free energy model with the newly estimated interaction parameters. Finally, we analyze the impact of feed molality, temperature, and staging on SDWE performance, focusing on water recovery, brine concentration, and required inlet DME to saline feed flow rate ratios. We conclude by examining the potential for DME-based SDWE to concentrate brines to the near-saturation levels required for minimal- and zero-liquid discharge applications and analyzing separation performance in salient limiting cases.

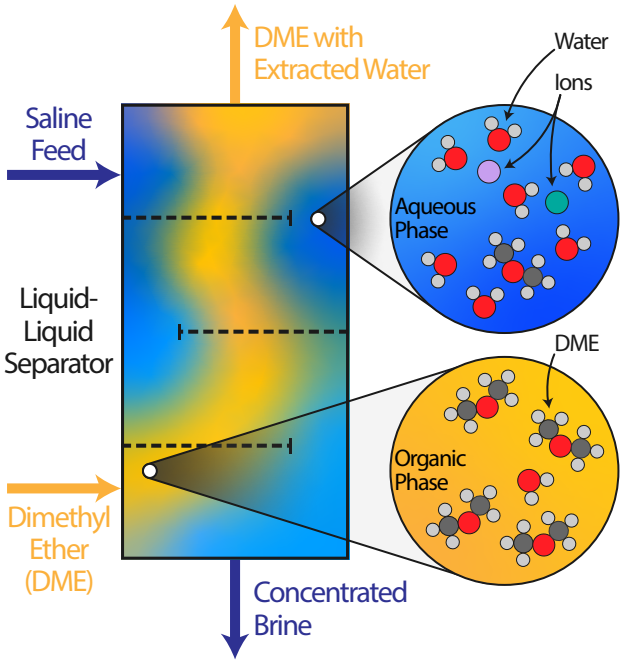

Figure 1: A schematic diagram of the liquid-liquid extraction system. The saline feed stream flows into the liquid-liquid separator where it is contacted with dimethyl ether (DME). The resulting water-dimethyl ether-sodium chloride mixture forms two distinct liquid phases: (1) an aqueous phase that exits the separator as the concentrated brine; and, (2) a DME-rich organic phase containing extracted water and negligible amounts of dissolved sodium chloride. The water-laden DME-rich stream passes to a solvent regeneration step for separation yielding desalinated water and DME, which is recycled into the separator.

2. Phase Equilibria in Water-Dimethyl Ether-Sodium Chloride Mixtures

In solvent-driven water extraction (SDWE) the saline feed water is mixed with dimethyl ether (DME) forming two liquid phases. A portion of the water from the saline feed is extracted into the DME-rich organic phase, while sodium chloride (NaCl) and other dissolved electrolytes remain in the aqueous phase. Quantifying the water recovery and brine concentration ratios attainable requires a rigorous understanding of the composition of the aqueous and organic liquid phases at each stage of the liquid-liquid separator (LLS). The composition of the aqueous (aq) and organic (org) phases at liquid-liquid equilibrium (LLE) at temperature T can be calculated by solving the isoactivity condition for each chemical species that is present in both liquid phases

$$\gamma_i^{\mathrm{aq}}\left(T, \boldsymbol{x}^{\mathrm{aq}}\right) x_i^{\mathrm{aq}} = \gamma_i^{\mathrm{org}}\left(T, \boldsymbol{x}^{\mathrm{org}}\right) x_i^{\mathrm{org}} \tag{1}$$

where x_i^p and γ_i^p are the mole fraction and activity coefficient of species i in phase p, respectively, and $\boldsymbol{x}^p$ is the mole fraction composition vector of phase p. The activity coefficient of

each species in each phase is calculated as a function of the mixture temperature and phase composition using an excess Gibbs free energy model (Section 2.1).

The regression of vapor-liquid and vapor-liquid-liquid equilibrium (VLE and VLLE, respectively) data can be used to augment LLE data in the estimation of interaction parameters for water–DME–NaCl mixtures. The VLE composition of the liquid (L) and vapor (V) phases at temperature T and pressure P can be calculated by solving the isofugacity condition for each volatile chemical species

$$\gamma_i^{\mathrm{L}}\left(T,\boldsymbol{x}^{\mathrm{L}}\right)x_i^{\mathrm{L}}P_i^{\mathrm{sat}}\left(T\right)\phi_i^{\mathrm{L,sat}}\left(T,P\right)=x_i^{\mathrm{V}}P\bar{\phi}_i^{\mathrm{V}}\left(T,P,\boldsymbol{x}^{\mathrm{V}}\right) \tag{2}$$

where ϕ_i^p is the fugacity coefficient of species i in phase p and the superscript sat represents saturation point for the pure component. The vapor-phase fugacity coefficient of water and DME is calculated as a function of the mixture's temperature, pressure, and vapor composition using an equation of state with mixing rules (Section 2.2).

2.1. Excess Gibbs Free Energy Model for Liquid-Liquid Equilibrium Calculations

The LIQUAC excess Gibbs free energy ($\underline{G}^{\mathrm{ex}}$) model is used to capture non-ideal behavior in liquid-phase water–DME–NaCl mixtures [39–50]. LIQUAC combines the UNIQUAC activity coefficient model for short-range interactions with a Pitzer-like electrolyte solution model for middle- and long-range interactions. The excess Gibbs free energy resulting from short-range interactions ($\underline{G}^{\mathrm{ex}}_{\mathrm{SR}}$) is [39, 44, 45, 50]

$$\frac{\underline{G}^{\mathrm{ex}}_{\mathrm{SR}}}{RT}=\sum_i x_i\ln\left(\frac{\phi_i}{x_i}\right)+\frac{z}{2}\sum_i q_i x_i\ln\left(\frac{\theta_i}{\phi_i}\right)-\sum_i q_i x_i\ln\left(\sum_j\theta_j\tau_{ji}\right) \tag{3}$$

where x_i is the mole fraction of species i; r_i and q_i denote the van der Waals volume and surface area parameters for species i, respectively; $\phi_i = x_i r_i/\sum_j x_j r_j$ and $\theta_i = x_i q_i/\sum_j x_j q_j$ denote the volume and area fractions of species i, respectively; z denotes the average coordination number of a molecule; and τ_{ji} is the normalized interaction energy parameter between species i and j. The middle-range contribution to $\underline{G}^{\mathrm{ex}}$, which encompasses cation-anion, ion-dipole, and ion-induced dipole interactions, is [40–43, 49, 51]

$$\frac{\underline{G}^{\mathrm{ex}}_{\mathrm{MR}}}{RT}=\sum_{i=1}^{N_{\mathrm{sol}}}\sum_{j=1}^{N_{\mathrm{ion}}}\left[B_{ij}\left(I_{\mathrm{m}}\right)x_i m_j\right]+x_{\mathrm{sol}}M_{\mathrm{sol}}\sum_{j_{\mathrm{c}}=1}^{N_{\mathrm{cation}}}\sum_{j_{\mathrm{a}}=1}^{N_{\mathrm{anion}}}\left[B_{j_{\mathrm{c}}j_{\mathrm{a}}}\left(I_{\mathrm{m}}\right)m_{j_{\mathrm{c}}}m_{j_{\mathrm{a}}}\right] \tag{4}$$

where M_{sol} is the molar mass of the uncharged solvent, m_i is the molality of species i, I_{m} is the ionic strength, B_{ij} is the interaction coefficient between uncharged species i and ion j, and $B_{j_{\mathrm{c}}j_{\mathrm{a}}}$ is the interaction coefficients between cation j_{c} and anion j_{a}. N_{sol}, N_{ion}, N_{cation},

and N_{anion} denote the total number of uncharged or solvent, ionic, cationic, and anionic species in the mixture, respectively. Ionic strength is defined as: $I_{\text{m}} = (1/2)\sum_{j=1}^{N_{\text{ion}}} m_j z_j^2$, where z_j is the charge number of ion j. Finally, the long-range contribution to $\underline{G}^{\text{ex}}$, which accounts for electrostatic forces between ions in the solvent medium, is given by the extended Debye-Hückel expression [52, 53]

$$\frac{\underline{G}^{\text{ex}}_{\text{LR}}}{RT} = -\frac{x_{\text{sol}} M_{\text{sol}} N_{\text{A}} \kappa}{3\epsilon_0 \epsilon_{\text{sol}} RT} \sum_{j=1}^{N_{\text{ion}}} m_j z_j^2 e^2 \tau\left(\kappa a\right) \tag{5}$$

where κ is the inverse Debye length, a is the distance of closest approach between ions, and τ is a function of the reduced Debye length (κa). Equation 5 can be approximated by: [40, 41, 54–56]

$$\frac{\underline{G}^{\text{ex}}_{\text{LR}}}{RT} = -\frac{4 x_{\text{sol}} M_{\text{sol}} A_{\text{DH}}}{b_{\text{DH}}^3}\left[\ln\left(1 + b_{\text{DH}}\sqrt{I_{\text{m}}}\right) - b_{\text{DH}}\sqrt{I_{\text{m}}} + \frac{b_{\text{DH}}^2 I_{\text{m}}}{2}\right] \tag{6}$$

where A_{DH} and b_{DH} are Debye-Hückel parameters. The Debye-Hückel parameters are a function of solvent mixture temperature (T), density (ρ_{sol}), and dielectric constant (ϵ_{sol}): $A_{\text{DH}} = k_{\text{DH}}^{(\text{A})}\sqrt{\rho_{\text{sol}}/(\epsilon_{\text{sol}} T)^3}$ and $b_{\text{DH}} = k_{\text{DH}}^{(\text{b})}\sqrt{\rho_{\text{sol}}/(\epsilon_{\text{sol}} T)}$. The constants $k_{\text{DH}}^{(\text{A})}$ and $k_{\text{DH}}^{(\text{b})}$ are 1.3278×10^5 mol$^{-0.5}$ m$^{1.5}$ K$^{1.5}$ and 6.3597 mol$^{-0.5}$ m$^{1.5}$ K$^{0.5}$, respectively. In this study, volume-averaged estimates for the solvent density and dielectric constant are used: $\rho_{\text{sol}} = \sum_i^{N_{\text{sol}}} v_i' \rho_i$ and $\epsilon_{\text{sol}} = \sum_i^{N_{\text{sol}}} v_i' \epsilon_i$, respectively, where v_i' is the salt-free volume fraction of solvent species i [57].

The rational activity coefficient (γ_i) of each species i, which is defined as: $RT\ln\gamma_i = (\partial N \underline{G}^{\text{ex}}/\partial N_i)_{T,P,N_{j\neq i}}$, can be expressed in terms of short-, middle-, and long-range contributions using Equations 3, 4, and 6 ,respectively. The short-range UNIQUAC-based contribution to γ_i is

$$\ln\gamma_i^{\text{SR}} = \ln\left(\frac{\phi_i}{x_i}\right) - \frac{z q_i}{2}\ln\left(\frac{\phi_i}{\theta_i}\right) + l_i - \frac{\phi_i}{x_i}\sum_j x_j l_j + q_i\left[1 - \ln\left(\sum_j \theta_j \tau_{ji}\right) - \sum_j\left(\frac{\theta_j \tau_{ji}}{\sum_j \theta_k \tau_{kj}}\right)\right] \tag{7}$$

where the parameter l_i is defined as: $l_i = [(r_i - q_i)\, z/2] - (r_i - 1)$. The normalized interaction energy parameter τ_{ji} is given by:

$$\ln\tau_{ji} = -\frac{\Delta u_{ji}}{RT} \approx \frac{a_{ji}^{(0)}}{T} + a_{ji}^{(1)} \tag{8}$$

where Δu_{ji} represents the difference in average interaction energy between the j-i and i-i species pairs, $a_{ji}^{(0)}$ and $a_{ji}^{(1)}$ are short-range interaction energy parameters that are determined

through the regression of experimental data, R denotes the universal gas constant, and T denotes absolute temperature of the mixture. The middle-range LIQUAC-based contribution to γ_i for solvent species is

$$\ln \gamma_i^{\mathrm{MR}} = \sum_{j=1}^{N_{\mathrm{ion}}} \left[B_{ij}\left(I_{\mathrm{m}}\right) m_j\right] - \left(\frac{M_i}{M_{\mathrm{sol}}}\right) \sum_{i=1}^{N_{\mathrm{sol}}} \sum_{j=1}^{N_{\mathrm{ion}}} \left\{\left[B_{ij}\big(I_{\mathrm{m}}\big) + I_{\mathrm{m}} B'_{ij}\big(I_{\mathrm{m}}\big)\right] x'_i m_j\right\} - M_i \sum_{j_{\mathrm{c}}=1}^{N_{\mathrm{cation}}} \sum_{j_{\mathrm{a}}=1}^{N_{\mathrm{anion}}} \left\{\left[B_{j_{\mathrm{c}}j_{\mathrm{a}}}\big(I_{\mathrm{m}}\big) + I_{\mathrm{m}} B'_{j_{\mathrm{c}}j_{\mathrm{a}}}\big(I_{\mathrm{m}}\big)\right] m_{j_{\mathrm{c}}} m_{j_{\mathrm{a}}}\right\} \tag{9}$$

Coefficients for middle-range solvent-ion and cation-anion interactions (B_{ij} and $B_{j_{\mathrm{c}}j_{\mathrm{a}}}$, respectively) are given by [40–43, 46, 48, 49, 51]

$$B_{ij} = b_{ij} + c_{ij} \exp\left(\alpha_{ij}^{(0)} \sqrt{I_{\mathrm{m}}} + \alpha_{ij}^{(1)} I_{\mathrm{m}}\right) \tag{10}$$

$$B_{j_{\mathrm{c}}j_{\mathrm{a}}} = b_{j_{\mathrm{c}}j_{\mathrm{a}}} + c_{j_{\mathrm{c}}j_{\mathrm{a}}} \exp\left(\alpha_{j_{\mathrm{c}}j_{\mathrm{a}}}^{(0)} \sqrt{I_{\mathrm{m}}} + \alpha_{j_{\mathrm{c}}j_{\mathrm{a}}}^{(1)} I_{\mathrm{m}}\right) \tag{11}$$

where b_{ij}, c_{ij}, $b_{j_{\mathrm{c}}j_{\mathrm{a}}}$, and $c_{j_{\mathrm{c}}j_{\mathrm{a}}}$ are middle-range interaction parameters that are determined through the regression of experimental data for each solvent-ion and cation-anion pair. The parameters $\alpha_{ij}^{(0)}$, $\alpha_{ij}^{(1)}$, $\alpha_{j_{\mathrm{c}}j_{\mathrm{a}}}^{(0)}$, and $\alpha_{j_{\mathrm{c}}j_{\mathrm{a}}}^{(1)}$ are fixed at -1.2, 0.25, -1.0, and 0.125, respectively [51]. The contribution of solvent-solvent, cation-cation, and anion-anion middle-range interactions are considered negligible. The long-range extended-Debye-Hückel contribution to γ_i for solvent species is [50, 53, 58, 59]

$$\ln \gamma_i^{\mathrm{LR}} = \frac{2 A_{\mathrm{DH}} M_i \rho_{\mathrm{sol}}}{b_{\mathrm{DH}}^3 \rho_i} \left[1 + b_{\mathrm{DH}} \sqrt{I_{\mathrm{m}}} - \frac{1}{1 + b_{\mathrm{DH}} \sqrt{I_{\mathrm{m}}}} - 2 \ln\left(1 + b_{\mathrm{DH}} \sqrt{I_{\mathrm{m}}}\right)\right] \tag{12}$$

2.2. Equation of State Model for Vapor-Liquid and Vapor-Liquid-Liquid Equilibrium Calculations

The Peng-Robinson Stryjek-Vera 2 (PRSV2) cubic equation of state combined with the van der Waals one-fluid mixing rule is used to model pressure-volume-temperature behavior of vapor- and liquid-phase water–DME mixtures, giving the vapor pressure (P) of a mixture in terms of its absolute temperature (T) and molar volume ($\underline{V}$) [50, 60–66]

$$P = \frac{RT}{\underline{V} - b_{\mathrm{mix}}} - \frac{a_{\mathrm{mix}}}{\underline{V}^2 + 2 b_{\mathrm{mix}} \underline{V} - b_{\mathrm{mix}}^2} \tag{13}$$

where R is the universal gas constant, while a_{mix} and b_{mix} are the molecular interaction and volume parameters of the mixture, respectively. Using the van der Waals one-fluid mixing rule, mixture parameters a_{mix} and b_{mix} are defined as: $a_{\mathrm{mix}} = \sum_i \sum_j x_i x_j a_{ij}$ and

$b_{\text{mix}} = \sum_i \sum_j x_i x_j b_{ij}$, respectively. The combining rules for a_{ij} and b_{ij} are: $a_{ij} = \sqrt{a_i a_j}(1 - k_{ij})$, where k_{ij} is the binary interaction energy parameter between species i and j, and $b_{ij} = (b_i + b_j)/2$, respectively. Using the PRSV2 equation of state, the fugacity coefficient of species i ($\bar{\phi}_i^p$) in the vapor- or liquid-phase p is given by [50, 60–63, 67]

$$\ln \bar{\phi}_i^p = \frac{b_i}{b_{\text{mix}}} \left(Z_{\text{mix}}^p - 1\right) - \ln\left(Z_{\text{mix}}^p - \frac{b_{\text{mix}} P}{RT}\right) - \frac{a_{\text{mix}}}{2\sqrt{2} b_{\text{mix}} RT} \left[\frac{2\sum_j (x_j a_{ij})}{a_{\text{mix}}} - \frac{b_i}{b_{\text{mix}}}\right] \ln\left[\frac{Z_{\text{mix}}^p + \left(1 + \sqrt{2}\right)\frac{b_{\text{mix}} P}{RT}}{Z_{\text{mix}}^p + \left(1 - \sqrt{2}\right)\frac{b_{\text{mix}} P}{RT}}\right] \tag{14}$$

where Z^p is the compressibility factor of phase p: $Z^p = P\underline{V}^p/(RT)$ (please see Appendix A). In this study, the PRSV2 parameters a and b for water and DME are taken from Stryjek and Vera [63] and k_{ij} is set to zero throughout.

3. Estimation of Excess Gibbs Free Energy Model Parameters

Expressions for the short- and middle-range contributions to the excess Gibbs free energy (Equations 7 and 9, respectively) contain interaction parameters that must be estimated through the regression of experimental data, predicted using group contribution methods [46, 48, 51, 68–70], or calculated from first-principles simulations [71–79]. In this work, experimental data from liquid-liquid, vapor-liquid, vapor-liquid-liquid equilibrium (LLE, VLE, and VLLE, respectively) is combined with osmotic coefficient measurements to determine the short- ($a_{ji}^{(0)}$ and $a_{ji}^{(1)}$ in Equation 7) and middle-range interaction parameters (b_{ij}, c_{ij}, $b_{j_c j_a}$, and $c_{j_c j_a}$ in Equation 9) in the LIQUAC model.

Regression is performed in three stages: (1) LLE, VLE, and VLLE data [80] is used to estimate H_2O–CH_3OCH_3 interaction parameters (Section 3.1); (2) osmotic coefficient data [81–83] is used to estimate H_2O–Na^+, H_2O–Cl^-, and Na^+–Cl^- parameters (Section 3.2); and, (3) LLE data [84] is used to estimate CH_3OCH_3–Na^+ and CH_3OCH_3–Cl^- parameters (please see Figure B.7 in Appendix B). In each stage, nonlinear least squares estimators are calculated using the generalized simulated annealing algorithm with local search for global optimization followed by the Broyden-Fletcher-Goldfarb-Shanno algorithm for local optimization implemented in Python using the SciPy package [44, 45, 85–92]. Previous studies have shown that fluid phase equilibrium calculations are relatively insensitive to the short-range interaction energy parameters between solvent-ion and cation-anion pairs [46, 48, 49]. Consequently, to reduce the number of estimated parameters and minimize the risk of overfitting, short-range interaction energy parameters between solvent-ion and cation-anion pairs are set to zero following the approach of Yan et al. [46], Kiepe et al. [48], and Zuend et al. [49].

LLE and VLE phase compositions are determined by solving Equations 1 and 2, respectively, for water and DME at a specified temperature and pressure. VLLE pressures and phase compositions are calculated by simultaneously solving Equation 1 for LLE between aqueous and organic liquid phases and Equation 2 for the VLE bubble point pressure between each liquid phase at its LLE composition and a common vapor phase at a specified temperature. In both isoactivity and isofugacity calculations, Equations 7, 9, and 12 are used to calculate water and DME activity coefficients as a function of mixture composition using estimated interaction parameters. Relative van der Waals surface area and volume parameters are either calculated using the UNIFAC group contribution method for water and DME molecules [93, 94] or taken from Mohs et al. [51] for sodium and chloride ions (please see Table B.6 in Appendix B). Vapor-phase fugacity coefficients for water and DME are calculated using Equation 14 for a specified temperature and pressure [50, 94]. Pure liquid-phase fugacity coefficients for water and DME at saturation are determined using Equation 14 with saturation pressures calculated as a function of temperature using the Design Institute for Physical Properties database [95]. Water and DME pure component acentric factors and characteristic κ parameters for the Peng-Robinson Stryjek-Vera 2 (PRSV2) equation of state are taken from Stryjek and Vera [63]. In each case, nonlinear equations are solved numerically using modified Powell's method implemented in Python using the SciPy package [85]. Expressions for the UNIQUAC, UNIFAC, and PRSV2 models use computer code from the Thermo package in Python [94].

3.1. Water-Dimethyl Ether Interaction Parameters

The nonlinear least squares estimators for short-range water–DME (H_2O–CH_3OCH_3) interaction energy parameters $\left(\boldsymbol{\theta}_1 = \left[a_{12}^{(0)}, a_{21}^{(0)}, a_{12}^{(1)}, a_{21}^{(1)}\right]\right)$ are calculated through the regression of LLE, VLE, and VLLE data for mixtures containing water and DME from Holldorff and Knapp [96]

$$\boldsymbol{\theta}_1 = \underset{\boldsymbol{\theta}_1' \in \mathbb{R}^4}{\operatorname{argmin}} \left\{ \sum_{k=1}^{n_{\text{aq}}^{\text{exp}}} \left[\frac{x_{\text{aq},k}^{\text{exp}} - x_{\text{aq},k}^{\text{mod}}\left(\boldsymbol{\theta}_1'\right)}{\sigma_{\text{aq},k}} \right]^2 + \sum_{k=1}^{n_{\text{org}}^{\text{exp}}} \left[\frac{x_{\text{org},k}^{\text{exp}} - x_{\text{org},k}^{\text{mod}}\left(\boldsymbol{\theta}_1'\right)}{\sigma_{\text{org},k}} \right]^2 + \sum_{k=1}^{n_{\text{VLE}}^{\text{exp}}} \left[\frac{P_{\text{VLE},k}^{\text{exp}} - P_{\text{VLE},k}^{\text{mod}}\left(\boldsymbol{\theta}_1'\right)}{\sigma_{\text{VLE},k}} \right]^2 + \sum_{k=1}^{n_{\text{VLLE}}^{\text{exp}}} \left[\frac{P_{\text{VLLE},k}^{\text{exp}} - P_{\text{VLLE},k}^{\text{mod}}\left(\boldsymbol{\theta}_1'\right)}{\sigma_{\text{VLLE},k}} \right]^2 \right\} \tag{15}$$

where σ represents the standard deviation of experimental uncertainties for a given measurement and the superscripts exp and mod denote experimentally-measured and model-calculated quantities. The standard deviation of experimental uncertainties in water–DME mixtures is set to 1.0×10^{-4} for aqueous and organic composition measurements (σ_{aq} and

σ_{org}, respectively) and 0.05 kPa for VLE and VLLE pressure measurements (σ_{VLE} and σ_{VLLE}, respectively), based on the bias uncertainty of the experimental apparatus used during data collection [80, 96].

3.2. Water-Sodium Chloride Interaction Parameters

The osmotic coefficient of solvent species i (ϕ_i^{osm}) can be calculated from its rational activity coefficient and the molality (m_j) of each ionic species j

$$\phi_i^{\text{osm}} = \frac{-\ln(\gamma_i x_i)}{M_i \sum_{j=1}^{N_{\text{ion}}} m_j} \tag{16}$$

where M_i is the molar mass of species i and N_{ion} is the number of ions in solution.

The nonlinear least squares estimators for middle-range water–Na^+, water–Cl^-, and Na^+–Cl^- interaction parameters ($\boldsymbol{\theta}_2 = [c_{13}, c_{14}, b_{34}, c_{34}]$) are calculated through the regression of osmotic coefficient data for mixtures containing water and NaCl from the Idaho Database of Solution Thermodynamics [81–83] and Partanen et al. [97, 98]

$$\boldsymbol{\theta}_2 = \underset{\boldsymbol{\theta}_2' \in \mathbb{R}^4}{\operatorname{argmin}} \left\{ \sum_{k=1}^{n_{\text{osm}}^{\text{exp}}} \left[\frac{\phi_{\text{aq},k}^{\text{osm,exp}} - \phi_{\text{aq},k}^{\text{osm,mod}}\left(\boldsymbol{\theta}_2'\right)}{\sigma_{\text{osm},k}} \right]^2 \right\} \tag{17}$$

The standard deviation of experimental uncertainties in water-NaCl mixtures is set to 0.001 for osmotic coefficient measurements (σ_{osm}) [81, 97, 98]. The LIQUAC expression for the excess Gibbs free energy of a single solvent mixture is independent of middle-range b_{ij} interaction parameters for solvent-ion pairs. Consequently, the middle-range interaction parameters b_{13} and b_{14}, which correspond to water–Na^+ and water–Cl^- interactions, respectively, cannot be estimated through the regression of osmotic coefficient data for water-NaCl mixtures.

3.3. Dimethyl Ether-Sodium Chloride Interaction Parameters

The nonlinear least squares estimators for middle-range DME–Na^+ and DME–Cl^- interaction parameters, along with the remaining subset of middle-range water–Na^+ and water–Cl^- parameters, ($\boldsymbol{\theta}_3 = [b_{13}, b_{14}, b_{23}, c_{23}, b_{24}, c_{24}]$) are calculated through the regression of LLE data for mixtures containing water, DME, and NaCl from McNally et al. [84]

$$\boldsymbol{\theta}_3 = \underset{\boldsymbol{\theta}_3' \in \mathbb{R}^6}{\operatorname{argmin}} \left\{ \sum_{k=1}^{n_{\text{aq}}^{\text{exp}}} \left[\frac{x_{\text{aq},k}^{\text{exp}} - x_{\text{aq},k}^{\text{mod}}\left(\boldsymbol{\theta}_1, \boldsymbol{\theta}_2, \boldsymbol{\theta}_3'\right)}{\sigma_{\text{aq},k}} \right]^2 \right\} \tag{18}$$

The standard deviation of experimental data for aqueous composition measurements (σ_{aq}) in water–DME–NaCl mixtures is set to 1.0×10^{-3} based on the experimental uncertainties of

the reported measurements [84]. Optimal values of previously calculated sets of water–DME, water–Na^+, and water–Cl^- interaction parameters ($\boldsymbol{\theta}_1$ and $\boldsymbol{\theta}_2$) are kept constant during the estimation of DME–Na^+ and DME–Cl^- interaction parameters ($\boldsymbol{\theta}_3$) using Equation 18. Experimental measurements demonstrate that the concentration of Na^+ and Cl^- ions in the organic phase of a water–DME–NaCl mixture at LLE is negligible as a result of the low polarity of DME (please see Appendix C). Consequently, LLE phase compositions for water–DME–NaCl mixtures can be calculated by solving Equation 1 for water and DME at a specified system temperature and aqueous-phase sodium chloride concentration.

3.4. Modeling Liquid-Liquid Equilibrium in Water-Dimethyl Ether-Sodium Chloride Mixtures with Estimated Interaction Parameters

Table 1 lists the nonlinear least squares estimates of the short- ($a_{ji}^{(0)}$ and $a_{ji}^{(1)}$ in Equation 7) and middle-range interaction parameters (b_{ij}, c_{ij}, $b_{j_c j_a}$, and $c_{j_c j_a}$ in Equation 9) determined through the regression of electrolyte fluid phase equilibria and osmotic coefficient data (Equations 15, 17, and 18). The parameters presented in Table 1 are incorporated into the LIQUAC excess Gibbs free energy model for fluid phase equilibria calculations throughout the remainder of this study.

Table 1: Short- and middle-range interaction parameters for the LIQUAC model estimated through the nonlinear regression of liquid-liquid, vapor-liquid, and vapor-liquid-liquid phase equilibrium (LLE, VLE, and VLLE, respectively) data for water–DME (Equation 15), osmotic coefficient data for water-NaCl (Equation 17), and LLE data for water–DME–NaCl mixtures (Equation 18).

Chemical Species		Short-Range Interaction Parameters			
i	j	$a_{ij}^{(0)}$ (K)	$a_{ji}^{(0)}$ (K)	$a_{ij}^{(1)}$	$a_{ji}^{(1)}$
H_2O	CH_3OCH_3	282.6	−798.6	−1.059	1.149
Chemical Species		**Middle-Range Interaction Parameters**			
i	j	b_{ij}		c_{ij}	
H_2O	Na^+	-2.514×10^{-2}		1.183×10^{-1}	
H_2O	Cl^-	-8.798×10^{-2}		-1.199×10^{-1}	
CH_3OCH_3	Na^+	-2.348×10^{-2}		1.671×10^{-1}	
CH_3OCH_3	Cl^-	5.662×10^{-3}		1.197×10^{-1}	
Na^+	Cl^-	1.699×10^{-1}		-2.267×10^{-1}	

Figure 2A shows the salt-free water mole fraction (x'_{H_2O}) in the aqueous (right-hand side) and organic phases (left-hand side) for a water–DME–NaCl mixture at LLE as a function of equilibrium temperature (T) for a range of aqueous-phase NaCl concentrations (x_{NaCl}). Aqueous- and organic-phase compositions are calculated using the LIQUAC excess Gibbs free energy model with NaCl mole fractions increasing from 0.00 (black curves) to 0.08 (lightest blue curves). The LIQUAC model, which reduces to UNIQUAC in the absence of

ionic species, effectively captures experimental LLE composition measurements for water–DME mixtures (black circles, Holldorff and Knapp [96]) across a temperature range from 250 K to 330 K with a mean absolute error (MAE) between the experimentally-measured and model-calculated water mole fractions of 5.9×10^{-3}. Figure 2B shows the aqueous-phase salt-free water mole fraction for a water–DME–NaCl mixture at LLE as a function of aqueous-phase NaCl concentration. Aqueous-phase compositions are calculated using the LIQUAC excess Gibbs free energy model at temperatures of 283 K (dark green curve), 298 K (green curve), and 313 K (light green curve). Part of the ternary diagram of the aqueous phase of the water–DME–NaCl mixture at LLE is shown in the Figure 2B Inset. The LIQUAC model accurately captures experimental LLE composition measurements for water–DME–NaCl mixtures (black diamonds, McNally et al. [84]) at a temperature of 298 K with a MAE between the experimental and modeled water mole fractions of 8.9×10^{-4}. Equilibrium calculations are performed treating Na^+ and Cl^- as separate species.

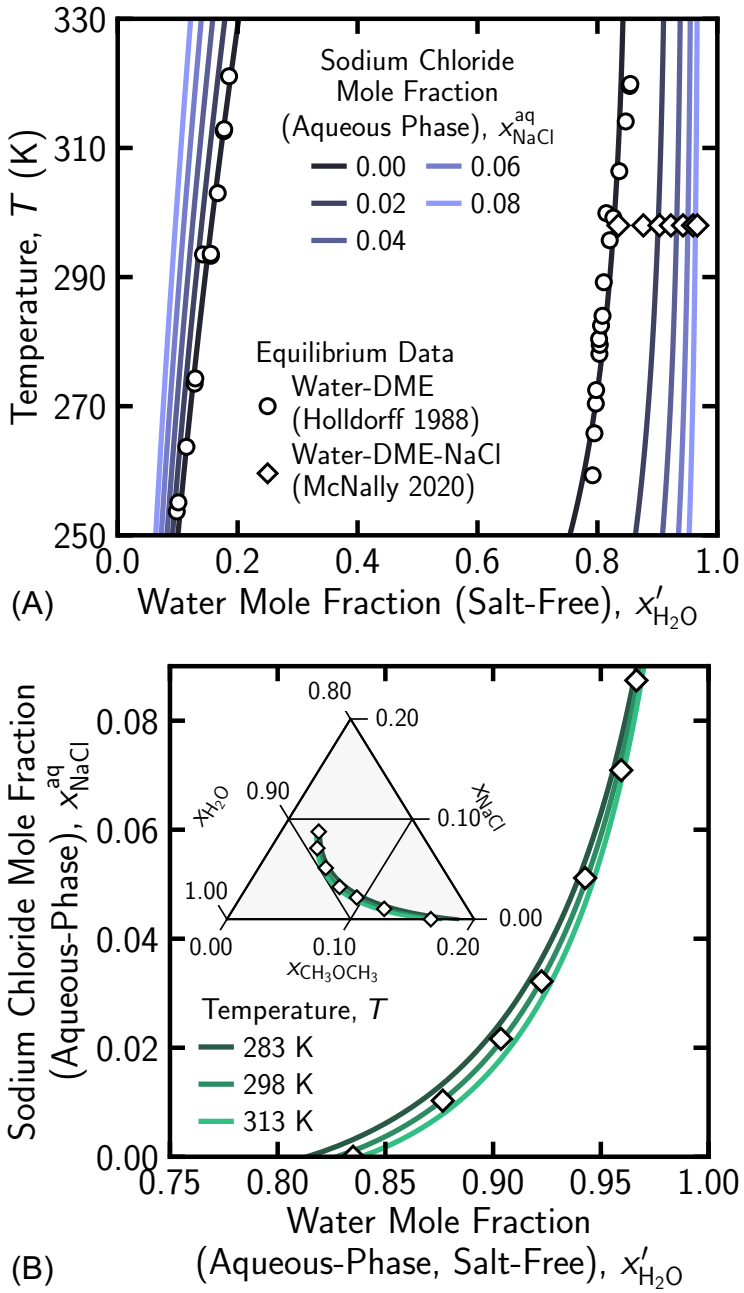

Figure 2: (A) Salt-free water mole fraction (x'_{H_2O}) in the aqueous (right hand side) and organic (left hand side) phases for a water–DME–NaCl mixture at liquid-liquid equilibrium (LLE) as a function of equilibrium temperature (T) for different aqueous-phase NaCl concentrations (x_{NaCl}). Water-DME mixture phase compositions (black curves) were determined using UNIQUAC parameters estimated from the nonlinear regression of fluid phase equilibria data (Table 1). Water-DME–NaCl mixture phase compositions (blue curves) were determined using LIQUAC parameters regressed from electrolyte fluid phase equilibria and osmotic coefficient data (Table 1). (B) Salt-free water mole fraction (x'_{H_2O}) in the aqueous phase of a water–DME–NaCl mixture at LLE as a function of aqueous-phase NaCl mole fraction (x^{aq}_{NaCl}) for different equilibrium temperatures (T). (B, Inset) Ternary diagram for the aqueous phase of a water–DME–NaCl mixture at LLE. Calculations are performed treating Na^+ and Cl^- as separate species.

The introduction of a salt can drastically alter the phase equilibria of a solvent mixture, particularly when its constituent ions interact preferentially with one solvent species relative to another [99]. Salts comprising small ions, such as NaCl, can interact strongly with highly polar solvents, such as water, enhancing solvent structure and lowering the chemical potential of more polar solvent species [100–107]. At equilibrium, a salt-driven reduction in the chemical potential of the more polar solvent species relative to the less polar species often leads to the enrichment of the more polar solvent in the salt-containing phase and its depletion from the fluid phase that does not contain salt [99]. Accurately quantifying the impact of ionic species on fluid phase equilibria in solvent mixtures is essential to calculating the water recovery attainable and the amount of solvent required for effective solvent-driven water extraction (SDWE) from hypersaline brines. The aqueous- and organic-phase water–DME–NaCl mixture phase compositions highlighted in this section are model calculated values determined using LIQUAC parameters estimated from fluid phase equilibria and osmotic coefficient data (Table 1).

Figure 2 highlights the pronounced impact of NaCl on LLE phase compositions in water–DME–NaCl mixtures. Adding NaCl to the water–DME–NaCl mixture leads to a rapid salting out of DME from the aqueous phase (Figure 2B). As the aqueous-phase NaCl mole fraction ($x^{\mathrm{aq}}_{\mathrm{NaCl}}$) is increased from 0.00 to 0.01, corresponding to a mixed-solvent NaCl molality ($m^{\mathrm{aq}}_{\mathrm{NaCl}}$) of 0.47 mol kg^{-1}, the aqueous-phase salt-free mole fraction of DME (x'_{DME}) decreases from 0.173 to 0.125. Further increasing $x^{\mathrm{aq}}_{\mathrm{NaCl}}$ from 0.01 to 0.04 (2.09 mol kg^{-1}) leads to a decrease in x'_{DME} to 0.068, while doubling $x^{\mathrm{aq}}_{\mathrm{NaCl}}$ from 0.04 to 0.08 (4.57 mol kg^{-1}) halves x'_{DME} to 0.037.

The salting out of DME from the aqueous phase drives a corresponding reduction in the organic-phase water mole fraction at LLE with increasing aqueous-phase NaCl mole fraction (Figure 2A). This decrease in the water content of the organic phase lowers the water recovery attainable as aqueous-phase salt concentration increases (Section 4). Increasing $x^{\mathrm{aq}}_{\mathrm{NaCl}}$ from 0.00 to 0.02 (0.98 mol kg^{-1}) leads to a reduction in $x'_{\mathrm{H_2O}}$ from 0.156 to 0.140 in the organic phase, which corresponds to a decrease in organic-phase salt-free water mass fraction ($w'_{\mathrm{H_2O}}$) from 0.067 to 0.060. Further increasing $x^{\mathrm{aq}}_{\mathrm{NaCl}}$ to 0.04 (2.09 mol kg^{-1}) lowers $x'_{\mathrm{H_2O}}$ to 0.125 or $w'_{\mathrm{H_2O}}$ to 0.053, while $x'_{\mathrm{H_2O}}$ and $w'_{\mathrm{H_2O}}$ decrease to 0.090 and 0.037, respectively, as $x^{\mathrm{aq}}_{\mathrm{NaCl}}$ is doubled to 0.08 (4.57 mol kg^{-1}).

Mixture temperature (T) has a comparatively moderate, though significant, impact on LLE phase compositions over the 250 K to 330 K range (Figure 2A). Higher solution temperatures drive an increase in the equilibrium water content of both the aqueous and organic phases. Unlike most binary mixtures that exhibit liquid-liquid phase separation, the aqueous and organic phase compositions at LLE of water–DME mixtures do not converge with

increasing temperature [108]. This anomalous aqueous-phase behavior in the 250 K to 330 K range may be caused by the directional hydrogen bonding between water and DME [108]. Simultaneously increasing the organic-phase water content and reducing the aqueous-phase DME content at LLE is highly advantageous in SDWE, maximizing water recovery while minimizing solvent loss. Increasing mixture temperature from 290 K to 320 K drives a 27% increase in the organic-phase salt-free water mole fraction from 0.146 to 0.187 in the absence of NaCl. The impact of temperature is maintained across higher aqueous-phase salt concentrations, with x'_{H_2O} increasing by 28% from 0.039 to 0.050 as T is increased from 290 K to 320 K for a x^{aq}_{NaCl} value of 0.08.

4. Water Extraction using a Multistage Counter-Current Liquid-Liquid Separator

Using the LIQUAC excess Gibbs free energy framework (Section 2) with interaction parameters estimated through the regression of experimental data (Section 3), a liquid-liquid separator (LLS) model is developed to quantify the performance of solvent-driven water extraction (SDWE). Figure 3A shows a schematic diagram of a counter-current LLS comprising n equilibrium or theoretical stages for the DME-driven desalination or concentration of high-salinity brines. The saline feed enters stage 1 forming the aqueous phase flowing from left to right. The water concentration in the aqueous stream decreases, while its salt concentration increases, in each stage of the LLS until it exits stage n as the concentrated brine. Similarly, DME enters stage n as the organic phase flowing from right to left. The water content of the DME-rich organic stream increases with each stage as water is transferred from the aqueous to the organic phase. Finally, the organic stream comprising DME and the extracted water exits the LLS from stage 1, passing to a solvent regeneration step. The aqueous-phase concentration of NaCl increases at each stage, though its molar flow rate remains constant given the negligible solubility of NaCl in the DME-rich organic phase. The aqueous and organic streams leaving each equilibrium or ideal stage are assumed to be in thermodynamic equilibrium, with the temperature (T) and pressure (P) constant across the LLS. Multistaging the counter-current LLS enables the water-laden organic stream to be contacted with an aqueous stream that is less saline than the final concentrated brine, enhancing the water recovery attainable for a given inlet DME to saline feed flow rate ratio [95]. Though detailed LLS process design calculations are beyond the scope of this study, the number of actual stages required typically scales with the number of equilibrium stages [95].

At steady state and in the absence of any chemical reactions, a molar flow rate balance

can be applied at each equilibrium or ideal stage a, giving

$$\dot{N}_{a-1}^{\mathrm{aq}} + \dot{N}_{a+1}^{\mathrm{org}} = \dot{N}_{a}^{\mathrm{aq}} + \dot{N}_{a}^{\mathrm{org}} \tag{19}$$

where $\dot{N}_a^p$ is the molar flow rate of the liquid phase p stream leaving stage a, following the leaving streams labeling convention. Superscripts aq and org denote properties of the aqueous and organic streams, respectively. Using Equation 1, chemical liquid-liquid equilibrium (LLE) between the aqueous and organic streams leaving each stage a gives

$$\gamma_{a,i}^{\mathrm{aq}} x_{a,i}^{\mathrm{aq}} = \gamma_{a,i}^{\mathrm{org}} x_{a,i}^{\mathrm{org}} \tag{20}$$

where $x_{a,i}^{\mathrm{aq}}$ and $\gamma_{a,i}^{\mathrm{aq}}$ are the mole fraction and activity coefficient, respectively, of species i, either water or DME, in the liquid phase p stream leaving stage a. For an n-stage countercurrent LLS, the molar flow rate and composition of the aqueous stream entering stage 1 ($\dot{N}_0^{\mathrm{aq}}$, $x_{0,\mathrm{H_2O}}^{\mathrm{aq}}$, $x_{0,\mathrm{DME}}^{\mathrm{aq}}$, and $x_{0,\mathrm{NaCl}}^{\mathrm{aq}}$) and the organic stream entering stage n ($\dot{N}_{n+1}^{\mathrm{org}}$, $x_{n+1,\mathrm{H_2O}}^{\mathrm{org}}$, and $x_{n+1,\mathrm{DME}}^{\mathrm{org}}$) are typically predefined. Given that NaCl remains in the aqueous phase, the NaCl concentration of the aqueous stream leaving each stage a ($x_{a,\mathrm{NaCl}}^{\mathrm{aq}}$) can be expressed in terms of its initial molar flow rate ($\dot{N}_{a,\mathrm{NaCl}}^{\mathrm{aq}}$): $x_{a,\mathrm{NaCl}}^{\mathrm{aq}} = \dot{N}_{0,\mathrm{NaCl}}^{\mathrm{aq}} x_{0,\mathrm{NaCl}}^{\mathrm{aq}} / \dot{N}_{a,\mathrm{NaCl}}^{\mathrm{aq}}$. The molar flow rates of the aqueous streams leaving each of the n stages, $\dot{\boldsymbol{N}}^{\mathrm{aq}} = \left[\dot{N}_1^{\mathrm{aq}}, \dot{N}_2^{\mathrm{aq}}, \ldots, \dot{N}_n^{\mathrm{aq}}\right]$, can be determined by solving the molar flow rate balance for water at each stage:

$$f_{\mathrm{H_2O}}\left(\begin{bmatrix}\dot{N}_1^{\mathrm{aq}}\\ \dot{N}_2^{\mathrm{aq}}\\ \vdots \\ \dot{N}_n^{\mathrm{aq}}\end{bmatrix}\right) = \begin{bmatrix} \dot{N}_0^{\mathrm{aq}} x_{0,\mathrm{H_2O}}^{\mathrm{aq}} + \dot{N}_2^{\mathrm{org}} x_{2,\mathrm{H_2O}}^{\mathrm{org}} - \dot{N}_1^{\mathrm{aq}} x_{1,\mathrm{H_2O}}^{\mathrm{aq}} - \dot{N}_1^{\mathrm{org}} x_{1,\mathrm{H_2O}}^{\mathrm{org}} \\ \dot{N}_1^{\mathrm{aq}} x_{1,\mathrm{H_2O}}^{\mathrm{aq}} + \dot{N}_3^{\mathrm{org}} x_{3,\mathrm{H_2O}}^{\mathrm{org}} - \dot{N}_2^{\mathrm{aq}} x_{2,\mathrm{H_2O}}^{\mathrm{aq}} - \dot{N}_2^{\mathrm{org}} x_{2,\mathrm{H_2O}}^{\mathrm{org}} \\ \vdots \\ \dot{N}_{n-1}^{\mathrm{aq}} x_{n-1,\mathrm{H_2O}}^{\mathrm{aq}} + \dot{N}_{n+1}^{\mathrm{org}} x_{n+1,\mathrm{H_2O}}^{\mathrm{org}} - \dot{N}_n^{\mathrm{aq}} x_{n,\mathrm{H_2O}}^{\mathrm{aq}} - \dot{N}_n^{\mathrm{org}} x_{n,\mathrm{H_2O}}^{\mathrm{org}} \end{bmatrix} = \mathbf{0} \tag{21}$$

where $f_{\mathrm{H_2O}} : \mathbb{R}^n \to \mathbb{R}^n$ is the stagewise water molar flow rate balance function. Equation 21 is solved numerically for $\dot{\boldsymbol{N}}^{\mathrm{aq}}$ using modified Powell's method implemented in Python using the SciPy package [85], incorporating the overall molar flow rate balance (Equation 19) and equilibrium conditions (Equation 20) at each stage. System-level calculations are performed by numerically solving for the input variable that satisfies a given target metric. For example, the inlet saline feed to DME molar flow rate ratio ($\dot{N}_{n+1}^{\mathrm{org}} / \dot{N}_0^{\mathrm{aq}}$) required to achieve a target organic-free outlet concentrated brine molality ($m_{\mathrm{NaCl}}^{\prime\,\mathrm{aq,out}\star}$) can be determined by solving

$$f_{m_{\mathrm{NaCl}}^{\prime\,\mathrm{aq,out}}}\left(\frac{\dot{N}_{n+1}^{\mathrm{org}}}{\dot{N}_0^{\mathrm{aq}}}\right) = \frac{x_{n,\mathrm{NaCl}}}{x_{n,\mathrm{H_2O}} M_{\mathrm{H_2O}}} - m_{\mathrm{NaCl}}^{\prime\,\mathrm{aq,out}\star} = 0 \tag{22}$$

where $f_{m_{\mathrm{NaCl}}^{\prime\,\mathrm{aq,out}}} : \mathbb{R}^1 \to \mathbb{R}^1$, and $M_{\mathrm{H_2O}}$ is the molar mass of water.

Figure 3B shows the normalized molar flow rate of water (blue shading), DME (yellow shading), and NaCl (green shading) in the aqueous (bottom row) and organic streams (top row) of a one- (left column), two- (middle column), and three-stage (right column) LLS. In each case, molar flow rates are normalized by the flow rate of the inlet saline feed stream ($\dot{N}_{\text{Feed}}^{\text{aq,in}}$ or $\dot{N}_{0}^{\text{aq}}$ using the leaving streams labeling notation). The inlet NaCl mole fraction ($x_{\text{NaCl}}^{\text{aq,in}}$ or $x_{0,\text{NaCl}}^{\text{aq}}$) and the inlet DME to feed molar flow rate ratio ($\dot{N}_{\text{DME}}^{\text{org,in}}/\dot{N}_{\text{Feed}}^{\text{aq,in}}$ or $\dot{N}_{n+1}^{\text{org}}/\dot{N}_{0}^{\text{aq}}$) are 0.040 (2.3 mol kg^{-1}) and 3.0, respectively. Equilibrium and molar flow rate calculations are performed treating Na^+ and Cl^- as separate species throughout this study. For the water–DME–NaCl mixtures studied, thermodynamic disequilibrium is greatest in the n^{th} or last stage, in which the organic stream comprising dry DME contacts the aqueous stream. The water concentration of the recycled DME entering the LLS ($x_{\text{H}_2\text{O}}^{\text{org,in}}$ or $x_{n+1,\text{H}_2\text{O}}^{\text{org}}$) is negligible, and thus a large amount of water is transferred from the aqueous to organic stream in the n^{th} stage, irrespective of the total number of stages. The organic stream continues to extract water as it flows from stage n to stage 1, though the amount of water transferred in each stage steadily decreases. Conversely, DME is rapidly transferred from the organic to aqueous stream in the first stage, where the saline feed, which has a DME concentration ($x_{\text{DME}}^{\text{aq,in}}$) of zero, contacts the DME-rich organic stream. For comparatively low- or moderate-salinity feed streams ($x_{\text{NaCl}}^{\text{aq,in}} < 0.040$ or $m_{\text{NaCl}}^{\text{aq,in}} < 2.3$ mol kg^{-1}), a portion of the DME that is transferred from the organic to aqueous stream in stage 1 is salted out by the increasing aqueous-phase NaCl concentration in subsequent stages and passes back into the organic stream. For high feed salinities ($x_{\text{NaCl}}^{\text{aq,in}} > 0.040$) the transfer of DME from the organic to aqueous stream is strongly limited by the high aqueous-phase NaCl concentration from the first equilibrium stage (Figure 3B).

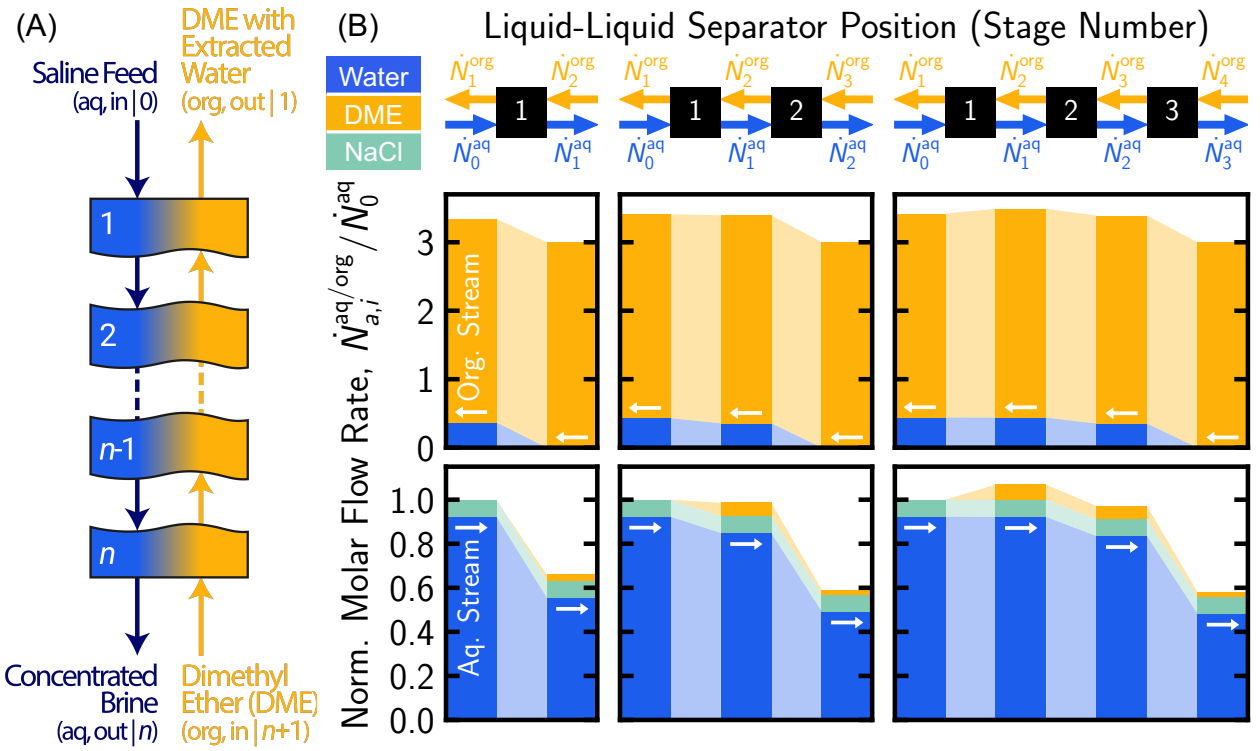

Figure 3: (A) Schematic diagram of a countercurrent multistage liquid-liquid separator. DME extracts water from the aqueous stream causing the mole fraction of water in the aqueous stream ($x_{a,\mathrm{H_2O}}^{\mathrm{aq}}$) to decrease from stage 1 to stage n, while the mole fraction of water in the organic stream ($x_{a,\mathrm{H_2O}}^{\mathrm{org}}$) increases from stage n to stage 1. (B) Normalized molar flow rate of water (blue bars), dimethyl ether (DME, yellow bars), and sodium chloride (NaCl, green bars) in the aqueous ($\dot{N}_{a,i}^{\mathrm{aq}}/\dot{N}_0^{\mathrm{aq}}$, bottom row, flowing left to right) and organic streams ($\dot{N}_{a,i}^{\mathrm{org}}/\dot{N}_0^{\mathrm{aq}}$, top row, flowing right to left) in a one- (left), two- (center), and three-stage (right) countercurrent separator. Shading represents the change in the normalized molar flow rate of species i across equilibrium stage a. The initial NaCl concentration ($x_{\mathrm{NaCl}}^{\mathrm{aq,in}}$ or $x_{0,\mathrm{NaCl}}^{\mathrm{aq}}$ using the leaving streams labeling notation) and the inlet DME to saline feed molar flow rate ratio ($\dot{N}_{\mathrm{DME}}^{\mathrm{org,in}}/\dot{N}_{\mathrm{Feed}}^{\mathrm{aq,in}}$ or $\dot{N}_{n+1}^{\mathrm{org}}/\dot{N}_0^{\mathrm{aq}}$) are 0.40 (2.3 mol kg^{-1}) and 3.0, respectively. Calculations are performed treating Na^+ and Cl^- as separate species.

5. Water Recovery and Brine Concentration in Solvent-Driven Water Extraction

The liquid-liquid separator (LLS) model developed in Section 4 allows key performance metrics for solvent-driven water extraction (SDWE), including the water recovery and brine concentration ratios, to be quantified and analyzed. Liquid-liquid equilibrium (LLE) calculations are performed using the LIQUAC excess Gibbs free energy model described in Section 2, incorporating interaction parameters estimated in Section 3 (Table 1). Figure 4 shows the water recovery ratio ($R_{\mathrm{H_2O}} = \dot{N}_{\mathrm{H_2O}}^{\mathrm{org,out}}/\dot{N}_{\mathrm{H_2O}}^{\mathrm{aq,in}}$, bars, primary axis) and extracted water to DME molar flow rate ratio ($\dot{N}_{\mathrm{H_2O}}^{\mathrm{org,out}}/\dot{N}_{\mathrm{DME}}^{\mathrm{org,out}} = x_{\mathrm{H_2O}}^{\mathrm{org,out}}/\left(1 - x_{\mathrm{H_2O}}^{\mathrm{org,out}}\right)$, diamonds, secondary axis) as a function of feed molality ($m_{\mathrm{NaCl}}^{\mathrm{aq,in}}$) and the inlet DME to saline feed molar flow rate ratio ($\dot{N}_{\mathrm{DME}}^{\mathrm{org,in}}/\dot{N}_{\mathrm{Feed}}^{\mathrm{aq,in}}$) for SDWE with a one-stage LLS (hatched bars and empty

diamonds). The increase in water recovery ratio attainable using a two-stage counter-current LLS (solid bars) and the water mole fraction in the organic stream leaving a two-stage LLS (filled diamonds) are also shown. The water recovery ratio is defined as the molar flow rate of water extracted by the organic stream ($\dot{N}^{\mathrm{org,out}}_{\mathrm{H_2O}}$ or $\dot{N}^{\mathrm{org}}_{1,\mathrm{H_2O}}$ using the leaving streams labeling notation) divided by the molar flow rate of water entering the LLS in the saline feed ($\dot{N}^{\mathrm{aq,in}}_{\mathrm{H_2O}}$ or $\dot{N}^{\mathrm{aq}}_{0,\mathrm{H_2O}}$). The inlet DME to saline feed molar flow rate ratio is defined as the molar flow rate of the organic stream, which contains DME only, entering the LLS in stage n ($\dot{N}^{\mathrm{org,in}}_{\mathrm{DME}}$ or $\dot{N}^{\mathrm{org}}_{n+1}$) divided by the molar flow rate of the saline feed, which contains water and NaCl, entering stage 1 ($\dot{N}^{\mathrm{aq,in}}_{\mathrm{Feed}}$ or $\dot{N}^{\mathrm{aq}}_{0}$). Feed molality ($m^{\mathrm{aq,in}}_{\mathrm{NaCl}}$) increases from 1.0 mol kg^{-1} (darkest bars and diamonds) to 2.5 mol kg^{-1} (lightest bars and diamonds), which corresponds to an increase in feed sodium chloride mole fraction ($x^{\mathrm{aq,in}}_{\mathrm{NaCl}}$) from 0.0177 to 0.0431.

Figure 4 highlights the potential for DME-based SDWE to achieve high water recovery ratios from high-salinity brines. For an inlet molality of 1.0 mol kg^{-1}, one-stage SDWE is able to achieve a water recovery ratio of 0.324 with an inlet DME to saline feed flow rate ratio of 2.0. Increasing the feed NaCl mole fraction leads to a small but sustained decrease in water recovery ratio as raising the aqueous-phase NaCl concentration in each stage drives a reduction in organic-phase water content at LLE (Figure 2A). As $m^{\mathrm{aq,in}}_{\mathrm{NaCl}}$ increases to 1.5 mol kg^{-1} (approximately 2.5 times the molality of seawater), $R_{\mathrm{H_2O}}$ drops to 0.309 with a $\dot{N}^{\mathrm{org,in}}_{\mathrm{DME}}/\dot{N}^{\mathrm{aq,in}}_{\mathrm{Feed}}$ of 2.0 for a one-stage extraction system. Further increasing $m^{\mathrm{aq,in}}_{\mathrm{NaCl}}$ to 2.0 mol kg^{-1} and 2.5 mol kg^{-1}, while keeping $\dot{N}^{\mathrm{org,in}}_{\mathrm{DME}}/\dot{N}^{\mathrm{aq,in}}_{\mathrm{Feed}}$ at 2.0, leads to an approximately linear reduction in $R_{\mathrm{H_2O}}$ to 0.293 and 0.278, respectively.

Increasing the inlet DME to saline feed flow rate ratio drives a significant increase in the attainable water recovery ratio. Increasing the molar flow rate of DME relative to the flow rate of the saline feed increases the equilibrium water-carrying capacity of the organic stream, enabling higher water recovery ratios. For example, for an $m^{\mathrm{aq,in}}_{\mathrm{NaCl}}$ of 2.5 mol kg^{-1}, which is over four times the salinity of seawater, a $\dot{N}^{\mathrm{org,in}}_{\mathrm{DME}}/\dot{N}^{\mathrm{aq,in}}_{\mathrm{Feed}}$ ratio of 4.0 can achieve a $R_{\mathrm{H_2O}}$ of 0.481 for one-stage SDWE, 73% higher than the water recovery ratio achieved with an $\dot{N}^{\mathrm{org,in}}_{\mathrm{DME}}/\dot{N}^{\mathrm{aq,in}}_{\mathrm{Feed}}$ of 2.0. For one-stage SDWE, the increase in $R_{\mathrm{H_2O}}$ with increasing $\dot{N}^{\mathrm{org,in}}_{\mathrm{DME}}/\dot{N}^{\mathrm{aq,in}}_{\mathrm{Feed}}$ is accompanied by a decrease in the extracted water to DME molar flow rate ratio ($\dot{N}^{\mathrm{org,out}}_{\mathrm{H_2O}}/\dot{N}^{\mathrm{org,out}}_{\mathrm{DME}}$). An increase in water recovery ratio leads to an increase in the NaCl mole fraction of the concentrated brine ($x^{\mathrm{aq,out}}_{\mathrm{NaCl}}$) causing a reduction in the extracted water mole fraction $x^{\mathrm{org,out}}_{\mathrm{H_2O}}$ at LLE (Figure 2A). A reduction in $\dot{N}^{\mathrm{org,out}}_{\mathrm{H_2O}}/\dot{N}^{\mathrm{org,out}}_{\mathrm{DME}}$ leads to an increase in the molar amount of organic solvent that must be regenerated and recycled per mole of water extracted. For an inlet feed molality of 1.0 mol kg^{-1}, doubling $\dot{N}^{\mathrm{org,in}}_{\mathrm{DME}}/\dot{N}^{\mathrm{aq,in}}_{\mathrm{Feed}}$ from 2.0 to 4.0, which yields a 84% increase in $R_{\mathrm{H_2O}}$, results in a decrease in $\dot{N}^{\mathrm{org,out}}_{\mathrm{H_2O}}/\dot{N}^{\mathrm{org,out}}_{\mathrm{DME}}$ from 0.162 to 0.145, increasing the moles of DME that must be recycled per mole of water

produced by 12%.

Figure 4 illustrates the significant role of staging in simultaneously increasing the water recovery and extracted water to DME molar flow rate ratios for a given feed molality and inlet DME to saline feed molar flow rate ratio. The impact of staging is more pronounced for higher R_{H_2O} values as both the aqueous and organic streams undergo a larger change in equilibrium state as they flow through the LLS. For an $m_{NaCl}^{aq,in}$ of 1.0 mol kg^{-1} and a $\dot{N}_{DME}^{org,in}/\dot{N}_{Feed}^{aq,in}$ of 2.0, a two-stage SDWE system increases the water recovery ratio by only 0.017 from 0.324 to 0.341 compared to a one-stage system. By contrast, when $\dot{N}_{DME}^{org,in}/\dot{N}_{Feed}^{aq,in}$ is 4.0, using a two-stage LLS yields a substantial increase in R_{H_2O} of 0.094 from 0.597, for a one-stage system, to 0.691 with an inlet molality of 1.0 mol kg^{-1}. In a LLS comprising a single equilibrium stage, the outflowing aqueous stream is in thermodynamic equilibrium with the outflowing organic stream leading to a trade-off between higher water recovery ratios and lower extracted water to DME molar flow rate ratios (Figure 3B). Staging the LLS largely decouples the positive impact of increasing $\dot{N}_{DME}^{org,in}/\dot{N}_{Feed}^{aq,in}$ on R_{H_2O} from its negative impact on $\dot{N}_{H_2O}^{org,out}/\dot{N}_{DME}^{org,out}$.

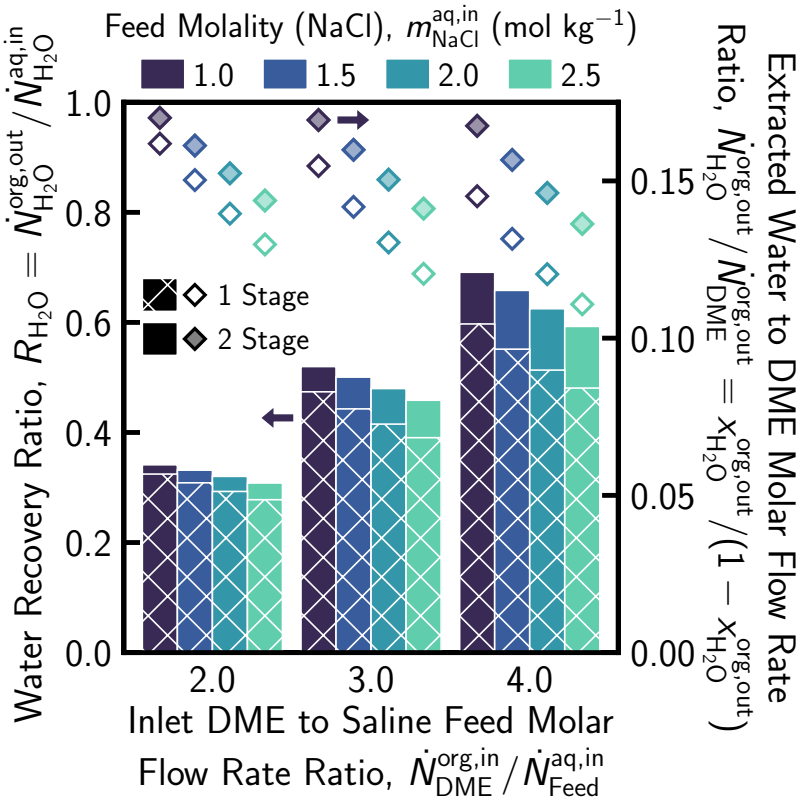

Figure 4: Water recovery ratio ($R_{H_2O} = \dot{N}_{H_2O}^{org,out}/\dot{N}_{H_2O}^{aq,in}$, bars, primary axis) and extracted water to DME molar flow rate ratio ($\dot{N}_{H_2O}^{org,out}/\dot{N}_{DME}^{org,out}$, diamonds, secondary axis) as a function of feed molality ($m_{NaCl}^{aq,in}$) and inlet dimethyl ether (DME) to saline feed molar flow rate ratio ($\dot{N}_{DME}^{org,in}/\dot{N}_{Feed}^{aq,in}$) for a one-stage (hatched bars and empty diamonds) and two-stage (solid bars and filled diamonds) counter-current liquid-liquid separator. Feed molality ($m_{NaCl}^{aq,in}$) increases from 1.0 mol kg^{-1} (darkest bars and diamonds) to 2.5 mol kg^{-1} (lightest bars and diamonds), which corresponds to an increase in feed sodium chloride mole fraction ($x_{NaCl}^{aq,in}$) from 0.0177 to 0.0431. System temperature (T) is fixed at 300 K. Calculations are performed treating Na^+ and Cl^- as separate species.

DME-based SDWE can concentrate saline feed streams to the near-saturation salinities that are required by minimal- and zero-liquid discharge (MLD and ZLD, respectively) processes. Figure 5 shows the inlet DME to saline feed molar flow rate ratio ($\dot{N}_{DME}^{org,in}/\dot{N}_{Feed}^{aq,in}$) required to reach representative MLD (left panel) and ZLD (right panel) outlet concentrated brine molalities ($m_{NaCl}^{\prime aq,out}$) of 4.0 mol kg^{-1} and 5.5 mol kg^{-1}, respectively, calculated on a organic-free basis, as a function of feed molality ($m_{NaCl}^{aq,in}$) for a one- (darker purple curves) and two-stage (lighter orange curves) counter-current LLS. The target $m_{NaCl}^{\prime aq,out}$ value of 5.5 mol kg^{-1} for ZLD processing is based on the saturation concentration of NaCl in the aqueous-phase of a water–DME–NaCl mixture [84]. System temperature is increased from 300 K (solid curves at the top edge of each shaded region) to 320 K (bottom edge). The water recovery ratio (R_{H_2O}, secondary axis) can be expressed as a function of organic-free inlet saline

feed and outlet concentrated brine molalities: $R_{H_2O} = 1 - \left(m_{NaCl}^{aq,in}/m_{NaCl}^{\prime aq,out}\right)$. The organic-free molality of the inlet saline feed is equal to its mixed-solvent molality ($m_{NaCl}^{\prime aq,in} = m_{NaCl}^{aq,in}$) as the saline feed stream does not contain DME.

Figure 5 demonstrates the potential for SDWE to reach the high brine salinities required for MLD and ZLD processes across a wide range of feed molalities. Calculating the amount of DME required to reach MLD and ZLD brine molalities, plays a central role in quantifying SDWE process performance and determining its feasibility compared to other brine desalination and concentration processes. In an SDWE system comprising a single equilibrium stage the outflowing aqueous stream, which forms the concentrated brine, is in thermodynamic equilibrium with the outflowing organic stream, which comprises DME and extracted water (Figure 3A). Consequently, the compositions of the aqueous and organic streams leaving a one-stage LLS are fixed for a given outlet concentrated brine molality ($m_{NaCl}^{\prime aq,out}$) and temperature (T). For an MLD $m_{NaCl}^{\prime aq,out}$ value of 4.0 mol kg^{-1}, the outlet extracted water mole fraction ($x_{H_2O}^{org,out}$) from a one-stage LLS is 0.109 at 300 K, rising to 0.126 at 320 K, irrespective of $m_{NaCl}^{aq,in}$. Similarly for one-stage SDWE with a ZLD $m_{NaCl}^{\prime aq,out}$ value of 5.5 mol kg^{-1}, $x_{H_2O}^{org,out}$ is fixed at 0.093 for a system temperature of 300 K and 0.108 at 320 K. As a result in one-stage SDWE, the required inlet DME to saline feed molar flow rate ratio decreases approximately linearly with feed molality $\dot{N}_{DME}^{org,in}/\dot{N}_{Feed}^{aq,in} = K_1[1 - (x_{Na^+}^{aq,in}/K_2)]$, where $x_{Na^+}^{aq,in} = m_{NaCl}^{aq,in}/\left[(1/M_{H_2O}) + 2m_{NaCl}^{aq,in}\right]$ (please see Appendix D). The constant K_1 decreases from 8.2 to 6.9 for $m_{NaCl}^{\prime aq,out} = 4.0$ mol kg^{-1} and from 9.8 to 8.3 for $m_{NaCl}^{\prime aq,out} = 5.5$ mol kg^{-1} as temperature is increased from 300 K to 320 K.

In a two-stage counter-current LLS, the outflowing aqueous and organic streams no longer leave the same equilibrium stage (Figure 3A), and, therefore, the outlet extracted water mole fraction ($x_{H_2O}^{org,out}$) can exceed values attained in a one-stage system. For high feed molality values ($m_{NaCl}^{aq,in}/m_{NaCl}^{\prime aq,out} > 0.8$), the water recovery is low ($R_{H_2O} < 0.2$) and the required inlet DME to saline feed molar flow rate ratio is similar for a one- and two-stage LLS as the thermodynamic state of the saline feed does not change significantly during the SDWE process. As $m_{NaCl}^{aq,in}$ decreases, the required $\dot{N}_{DME}^{org,in}/\dot{N}_{Feed}^{aq,in}$ for a two-stage LLS increases more gradually compared to a one-stage LLS. For example, for a $m_{NaCl}^{aq,in}$ of 2.0 mol kg^{-1}, the $\dot{N}_{DME}^{org,in}/\dot{N}_{Feed}^{aq,in}$ required for two-stage SDWE operating at 300 K is 3.82 and 4.33 for MLD and ZLD target $m_{NaCl}^{\prime aq,out}$ values of 4.0 mol kg^{-1} and 5.5 mol kg^{-1}, respectively. These $\dot{N}_{DME}^{org,in}/\dot{N}_{Feed}^{aq,in}$ values represent a 26% and 33% reduction compared to one-stage SDWE for MLD and ZLD, respectively. Reducing $m_{NaCl}^{aq,in}$ further leads to a plateau in the inlet DME to saline feed molar flow rate ratio as the impact of increasing the water recovery ratio, which drives an increase in $\dot{N}_{DME}^{org,in}/\dot{N}_{Feed}^{aq,in}$, is balanced by the increase in extracted water mole fraction, which lowers $\dot{N}_{DME}^{org,in}/\dot{N}_{Feed}^{aq,in}$. As $m_{NaCl}^{aq,in}$ is reduced to 0.0 mol kg^{-1}, $\dot{N}_{DME}^{org,in}/\dot{N}_{Feed}^{aq,in}$

approaches: $(1/x_{H_2O}^{org,bin}) - 1$, where $x_{H_2O}^{org,bin}$ is the organic-phase water mole fraction in a binary water–DME mixture at LLE (left-hand side black curve in Figure 2A), corresponding to 5.29 at 300 K and 4.35 at 320 K. In the $m_{NaCl}^{aq,in} \rightarrow 0.0$ mol kg^{-1} limit, $\dot{N}_{DME}^{org,in}/\dot{N}_{Feed}^{aq,in}$ is independent of $m_{NaCl}^{\prime aq,out}$ and the number of stages (n), provided that $n \geqslant 2$, as the majority of mass transfer occurs in the final stages (Figure 3B) and, thus, the NaCl mole fraction in the aqueous stream leaving the first stage is negligible (please see Appendix D). Though DME-based SDWE is able to reach the concentrated brine salinities required for MLD and ZLD, the process is most effective when treating highly-saline feed streams ($m_{NaCl}^{aq,out} > 2.0$ mol kg^{-1}, over three times the salinity of seawater) as the amount of DME required increases rapidly for less saline feed streams.

Increasing system temperature yields a significant reduction in the required inlet DME to saline feed molar flow rate ratio across a range of feed molalities for both one- and two-stage SDWE systems. Raising T leads to an increase in the organic-phase water mole fraction at LLE (left-hand side curves in Figure 2A), which drives an increase in $x_{H_2O}^{org,out}$ and, ultimately, a monotonic reduction in $\dot{N}_{DME}^{org,in}/\dot{N}_{Feed}^{aq,in}$. For example, for $m_{NaCl}^{aq,in} = 2.0$ mol kg^{-1} and a target MLD $m_{NaCl}^{\prime aq,out}$ value of 4.0 mol kg^{-1}, increasing T from 300 K to 320 K yields a 15% reduction in $\dot{N}_{DME}^{org,in}/\dot{N}_{Feed}^{aq,in}$ from 5.18 to 4.39 for a one-stage LLS and a 16% reduction in $\dot{N}_{DME}^{org,in}/\dot{N}_{Feed}^{aq,in}$ from 3.82 to 3.21 for a two-stage system. For water–DME–NaCl mixtures, increasing T leads to a reduction, rather than an increase, in the aqueous-phase DME mole fraction at LLE (Figure 2), reducing the amount of DME lost in outflowing aqueous stream. Consequently, increasing system temperature has uniformly positive impact on $\dot{N}_{DME}^{org,in}/\dot{N}_{Feed}^{aq,in}$.

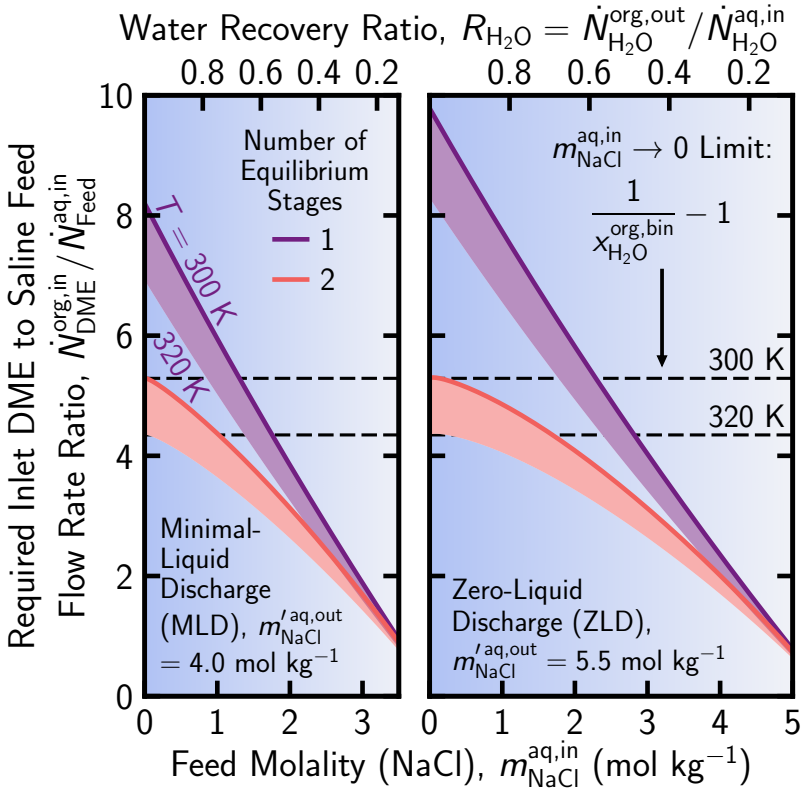

Figure 5: Required inlet dimethyl ether (DME) to saline feed molar flow rate ratio ($\dot{N}^{org,in}_{DME}/\dot{N}^{aq,in}_{Feed}$) for a minimum-liquid discharge (MLD, left) and zero-liquid discharge (ZLD, right) process as a function of feed molality ($m^{aq,in}_{NaCl}$) for a one-stage (darker purple curves) and two-stage (lighter orange curves) counter-current liquid-liquid separator. MLD and ZLD processes are defined as having an outlet concentrated brine molality ($m'^{aq,out}_{NaCl}$) of 4.0 mol kg^{-1} and 5.5 mol kg^{-1}, respectively, calculated on a organic-free basis. System temperature increases from 300 K (solid curve at the top edge of each shaded region) to 320 K (bottom edge). The values of $\dot{N}^{org,in}_{DME}/\dot{N}^{aq,in}_{Feed}$ in the limit as $m^{aq,in}_{NaCl} \to 0$ mol kg^{-1} are indicated for system temperatures of 300 K and 320 K (black dashed lines). Calculations are performed treating Na^+ and Cl^- as separate species.

Brine concentration and volume reduction play an important role in minimizing the costs associated with brine disposal while promoting efficacious brine valorization. Figure 6 shows the organic-free saline feed to concentrated brine salt concentration ratio ($m'^{aq,out}_{NaCl}/m^{aq,in}_{NaCl}$, panel A) and the extracted water to DME molar flow rate ratio ($\dot{N}^{org,out}_{H_2O}/\dot{N}^{org,out}_{DME}$, panel B) as a function of feed molality ($m^{aq,in}_{NaCl}$) and the inlet DME to saline feed molar flow rate ratio ($\dot{N}^{org,in}_{DME}/\dot{N}^{aq,in}_{Feed}$) for SDWE with a one-stage LLS. As the solubility of NaCl in the organic phase is negligible, the extracted water to DME molar flow rate ratio can be expressed in terms of the extracted water mole fraction ($x^{org,out}_{H_2O}$): $\dot{N}^{org,out}_{H_2O}/\dot{N}^{org,out}_{DME} = x^{org,out}_{H_2O}/\left(1 - x^{org,out}_{H_2O}\right)$. The increase in $m'^{aq,out}_{NaCl}/m^{aq,in}_{NaCl}$ and $\dot{N}^{org,out}_{H_2O}/\dot{N}^{org,out}_{DME}$ attainable using two-stage SDWE relative to a one-stage system is indicated on their respective panels (white contour lines). The feed sodium chloride mole fraction (secondary axis) is given by: $x^{aq,in}_{NaCl} = m^{aq,in}_{NaCl}/\left[\left(1/M_{H_2O}\right) +\right.$

$m_{\mathrm{NaCl}}^{\mathrm{aq,in}}$]. System temperature is fixed at 300 K throughout.

Figure 6A illustrates the high saline feed to concentrated brine salt concentration ratios attainable by SDWE across a wide range of feed molalities. The salt concentration ratio calculated on an organic-free basis ($m_{\mathrm{NaCl}}^{\prime\mathrm{aq,out}}/m_{\mathrm{NaCl}}^{\mathrm{aq,in}}$) is inversely proportional to the water molar or mass flow rate reduction ratio ($\dot{N}_{\mathrm{H_2O}}^{\mathrm{aq,out}}/\dot{N}_{\mathrm{H_2O}}^{\mathrm{aq,in}}$ or $\dot{M}_{\mathrm{H_2O}}^{\mathrm{aq,out}}/\dot{M}_{\mathrm{H_2O}}^{\mathrm{aq,in}}$, respectively) achieved by an SDWE system. At the lower end of the feed salinity spectrum, a one-stage LLS is able to achieve a $m_{\mathrm{NaCl}}^{\prime\mathrm{aq,out}}/m_{\mathrm{NaCl}}^{\mathrm{aq,in}}$ ratio of 2.5 with $m_{\mathrm{NaCl}}^{\mathrm{aq,in}} = 1.0$ mol kg^{-1} and an inlet DME to saline feed molar flow rate ratio of 4.0. For a highly-saline feed stream with a feed molality of 3.0 mol kg^{-1}, one-stage SDWE can achieve a salt concentration ratio of 2.0 with a $\dot{N}_{\mathrm{DME}}^{\mathrm{org,in}}/\dot{N}_{\mathrm{Feed}}^{\mathrm{aq,in}}$ of 5.0, taking the NaCl concentration in the outflowing aqueous stream close to saturation. Salt concentration ratios decrease with increasing $m_{\mathrm{NaCl}}^{\mathrm{aq,in}}$ as the corresponding increase in $x_{\mathrm{NaCl}}^{\mathrm{aq}}$ in each stage lowers the water-content of the organic phase at LLE (Figure 2A). Increasing $\dot{N}_{\mathrm{DME}}^{\mathrm{org,in}}/\dot{N}_{\mathrm{Feed}}^{\mathrm{aq,in}}$ rapidly increases the amount of water extracted as the aqueous and organic streams equilibrate, driving an increase in $m_{\mathrm{NaCl}}^{\prime\mathrm{aq,out}}/m_{\mathrm{NaCl}}^{\mathrm{aq,in}}$.

Maximizing the extracted water to DME molar flow rate ratio ($\dot{N}_{\mathrm{H_2O}}^{\mathrm{org,out}}/\dot{N}_{\mathrm{DME}}^{\mathrm{org,out}}$) or extracted water mole fraction ($x_{\mathrm{H_2O}}^{\mathrm{org,out}}$) minimizes the moles of DME that must be regenerated and recycled for every mole of desalinated water produced. Higher $\dot{N}_{\mathrm{H_2O}}^{\mathrm{org,out}}/\dot{N}_{\mathrm{DME}}^{\mathrm{org,out}}$ lower both the energy consumption and size of the DME regeneration system that separates the extracted water from the DME, recycling the latter back into the LLS. Figure 6B shows that increasing either $m_{\mathrm{NaCl}}^{\mathrm{aq,in}}$ or $\dot{N}_{\mathrm{DME}}^{\mathrm{org,in}}/\dot{N}_{\mathrm{Feed}}^{\mathrm{aq,in}}$ has a negative impact on $\dot{N}_{\mathrm{H_2O}}^{\mathrm{org,out}}/\dot{N}_{\mathrm{DME}}^{\mathrm{org,out}}$ for one-stage SDWE. Increasing $m_{\mathrm{NaCl}}^{\mathrm{aq,in}}$ or $\dot{N}_{\mathrm{DME}}^{\mathrm{org,in}}/\dot{N}_{\mathrm{Feed}}^{\mathrm{aq,in}}$ lead to an increase in the molality of the outflowing aqueous stream ($m_{\mathrm{NaCl}}^{\prime\mathrm{aq,out}}$), which results in a reduction in the water content of the outflowing organic stream at LLE. Multistaging the LLS weakens the negative impact of high $m_{\mathrm{NaCl}}^{\prime\mathrm{aq,out}}$ values on $x_{\mathrm{H_2O}}^{\mathrm{org,out}}$. Consequently, using a multistage LLS partially overcomes the trade-off between high saline feed to concentrated brine salt concentration ratios and low extracted water to DME molar flow rate ratios. For feed molality values and inlet DME to saline feed molar ratios higher than 2.0 mol kg^{-1} and 4.0, respectively, using a two-stage system can simultaneously increase $m_{\mathrm{NaCl}}^{\prime\mathrm{aq,out}}/m_{\mathrm{NaCl}}^{\mathrm{aq,in}}$ by 25% and $\dot{N}_{\mathrm{H_2O}}^{\mathrm{org,out}}/\dot{N}_{\mathrm{DME}}^{\mathrm{org,out}}$ by 20%.

Excessive solvent loss can hamper the effectiveness of SDWE systems, increasing cost and requiring additional post-treatment steps to remove residual solvent from the concentrated brine stream. Maximizing the DME recovery ratio ratio ($R_{\mathrm{DME}} = \dot{N}_{\mathrm{DME}}^{\mathrm{org,out}}/\dot{N}_{\mathrm{DME}}^{\mathrm{org,in}}$) ensures that solvent costs are kept to a minimum while minimizing the need for extensive post-treatment. DME-based SDWE is able to achieve solvent recovery ratios of greater than 0.98 across a wide range of feed molalities ($m_{\mathrm{NaCl}}^{\mathrm{aq,in}} > 1.0$ mol kg^{-1}) and inlet DME to saline feed molar flow rate ratios ($\dot{N}_{\mathrm{DME}}^{\mathrm{org,in}}/\dot{N}_{\mathrm{Feed}}^{\mathrm{aq,in}} > 2.5$) without additional separations steps (please see Appendix E). Indeed, increasing $m_{\mathrm{NaCl}}^{\mathrm{aq,in}}$ and $\dot{N}_{\mathrm{DME}}^{\mathrm{org,in}}/\dot{N}_{\mathrm{Feed}}^{\mathrm{aq,in}}$ drives an increase in R_{DME} as DME

is salted out from the aqueous phase of a water–DME–NaCl mixture at LLE (Figure E.9).

The equilibrium model developed in this study highlights the potential for DME-based SDWE to treat hypersaline brines, achieving high water recovery (Figures 4 and 5) and brine concentration ratios (Figure 6A). The required inlet DME to feed flow rate ratios and the number of equilibrium stages calculated in this work are important practical design parameters for various LLS configurations, including mixer-settlers, packed columns, and spray columns [95, 109, 110]. Combined with the density difference and interfacial tension between liquid phases, the parameters calculated in this study are central to the design and sizing of LLS process equipment [95, 109, 110]. Further work is required to understand the mass transfer between the aqueous and organic phases and the rate of phase separation in water–DME–NaCl mixtures. For example, experimental measurements are needed to determine the interfacial tension between the aqueous and organic phases of a water–DME–NaCl mixture, which controls the phase separation rate, as a function of temperature and NaCl concentration. Furthermore, an effective DME regeneration and recycling system must be conceptualized to estimate the energy efficiency of SDWE.

Coupled with an energy-efficient solvent regeneration system, DME-driven SDWE has several practical applications ranging from hypersaline brine desalination for the concentration of industrial wastewater to fractional precipitation for the enhanced recovery and recycling of critical energy materials. At the molecular scale, further research is required to understand the fluid phase equilibrium behavior of a broader range of aqueous-organic-electrolyte mixtures, including multi-electrolyte mixtures [70, 111–113]. In particular, a combined experimental and theoretical approach is needed to study the solvation of highly concentrated electrolytes in multi-solvent solutions [114]. At the system scale, additional work is needed to calculate energy consumption, size process equipment, and, ultimately, estimate the cost and environmental footprint of SDWE systems.

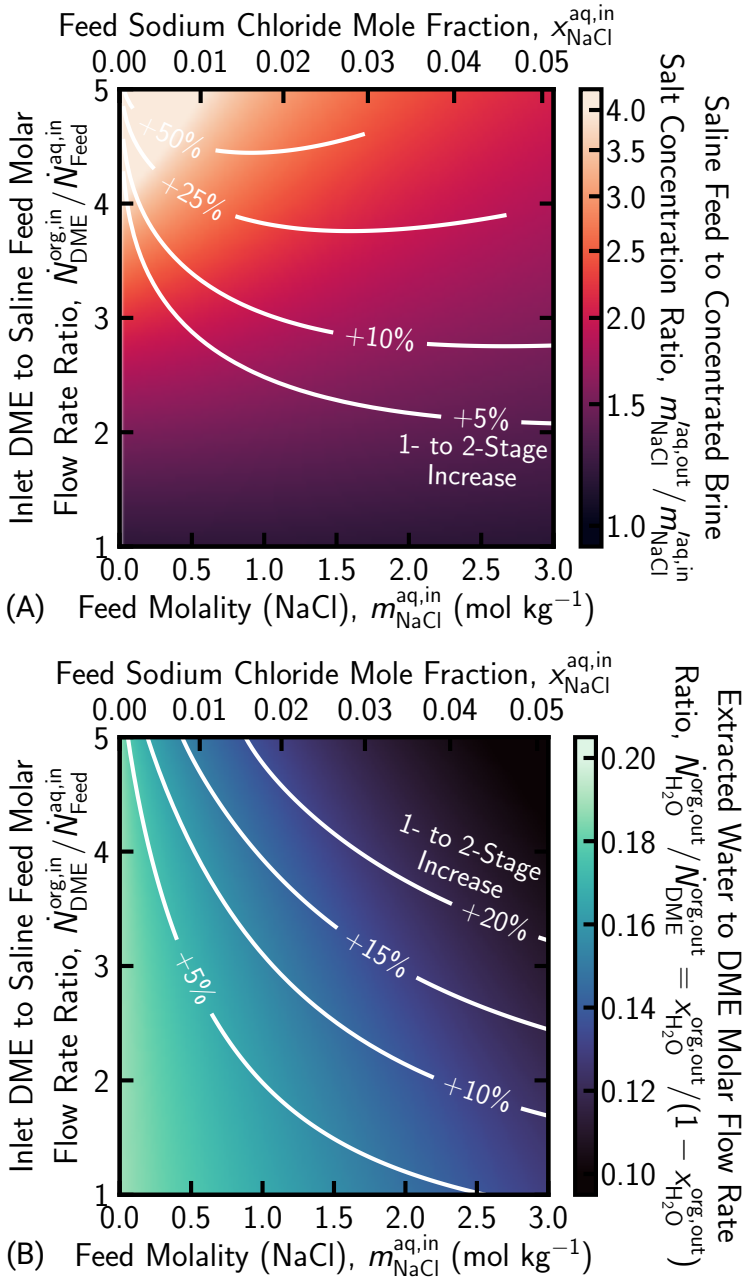

Figure 6: (A) Salt concentration factor ($m'^{aq,out}_{NaCl}/m^{aq,in}_{NaCl}$) as a function of feed molality ($m^{aq,in}_{NaCl}$) and inlet DME to saline feed molar flow rate ratio ($\dot{N}^{org,in}_{DME}/\dot{N}^{aq,in}_{Feed}$) for one-stage solvent-driven water extraction (SDWE). Concentration factors ($m'^{aq,out}_{NaCl}/m^{aq,in}_{NaCl}$) are calculated on a organic-free basis and system temperature (T) is fixed at 300 K. Contour lines (white curves) indicate the increase in $m'^{aq,out}_{NaCl}/m^{aq,in}_{NaCl}$ achieved by increasing the number of equilibrium or theoretical counter-current liquid-liquid separator stages from one to two. Contour lines are truncated for high $x^{aq,in}_{NaCl}$ and $\dot{N}^{org,in}_{DME}/\dot{N}^{aq,in}_{Feed}$ values as sodium chloride saturation is reached in two-stage SDWE. The feed sodium chloride mole fraction is given by: $x^{aq,in}_{NaCl} = m^{aq,in}_{NaCl}/\left[(1/M_{H_2O}) + m^{aq,in}_{NaCl}\right]$.

Figure 6: [Continued] (B) Extracted water to DME molar flow rate ratio ($\dot{N}_{H_2O}^{org,out}/\dot{N}_{DME}^{org,out}$) as a function of feed molality ($m_{NaCl}^{aq,in}$) and inlet DME to saline feed molar flow rate ratio ($\dot{N}_{DME}^{org,in}/\dot{N}_{Feed}^{aq,in}$) for one-stage SDWE. System temperature is fixed at 300 K. Contour lines (white curves) indicate the increase in $\dot{N}_{H_2O}^{org,out}/\dot{N}_{DME}^{org,out}$ achieved by increasing the number of equilibrium stages from one to two. The feed sodium chloride mole fraction is given by: $x_{NaCl}^{aq,in} = m_{NaCl}^{aq,in}/\left[\left(1/M_{H_2O}\right) + m_{NaCl}^{aq,in}\right]$. Calculations are performed treating Na^+ and Cl^- as separate species.

6. Conclusions

Solvent-driven water extraction (SDWE) using dimethyl ether (DME) has the potential to desalinate or concentrate aqueous feed streams, playing an important role in minimal- or zero-liquid discharge processing and enhanced resource recovery. Mass transfer in SDWE occurs at a liquid-liquid interface between an aqueous and organic phase, partially negating the detrimental impact of scaling and fouling on critical membrane and heat transfer surfaces in many desalination systems. In the preceding analysis, we develop an equilibrium-based liquid-liquid separator (LLS) model to explore the potential for hypersaline brine desalination using SDWE for the first time.

We begin by building a computational platform based on the LIQUAC model, which combines the UNIQUAC model for short-range interactions with a Pitzer-like electrolyte solution model for middle- and long-range interactions, to calculate the excess Gibbs free energy ($\underline{G}^{ex}$) of water–DME–NaCl mixtures. Nonlinear least squares estimators for LIQUAC interaction parameters are calculated through the regression of fluid phase equilibrium and osmotic coefficient data. DME–Na^+ and DME–Cl^- interaction parameters are estimated for the first time using recently published liquid-liquid equilibrium (LLE) data for water–DME–NaCl mixtures. The LIQUAC $\underline{G}^{ex}$ model is then incorporated into an equilibrium-based computational model of a multistage counter-current LLS to calculate the water recovery and brine concentration ratios attainable by SDWE using DME.

Using the LLS model we demonstrate that DME-based SDWE has the potential to desalinate high-salinity brines achieving high water recoveries. For example, with a feed molality of 2.5 mol kg^{-1} (over four times the salinity of seawater), we show that a one-stage LLS yields a water recovery ratio (R_{H_2O}) of 0.48 with an inlet DME to saline feed molar flow rate ratio of 4.0 at 300 K, with R_{H_2O} increasing to 0.59 for two-stage SDWE. Our analysis illustrates that SDWE is able to reach the high concentrated brine salinities required for minimal- or zero-liquid discharge for feed molalities ranging from 0.0 mol kg^{-1} to 5.0 mol kg^{-1} and quantifies the amount of DME required. Finally, we highlight the importance of staging in overcoming the trade-off between increasing water recovery ratio and reducing extracted water mole fraction. The computational framework developed in this work enables the separa-

tion performance of DME-based SDWE to be quantified for the first time. The methodology formulated and the key limiting cases identified provide a platform for the analysis of other solvents and electrolytes. The promising water recovery and brine concentration ratios attainable using SDWE motivate future work examining mass transfer between liquid phases in aqueous-organic-electrolyte mixtures and developing efficient solvent regeneration systems.

Acknowledgment

This work was supported by the United States Department of Energy through contract DE-AC07-05ID14517. Funding was supplied by Idaho National Laboratory via the Laboratory Directed Research and Development Fund (LDRD).

Nomenclature

Roman Letters:

$a_{ij}^{(0)}$	(K)	UNIQUAC short-range interaction energy parameter between species i and j
$a_{ij}^{(1)}$		First-order expansion of UNIQUAC short-range interaction energy parameter between species i and j in temperature
a_{mix}	(J kmol^{-1})	Peng-Robinson mixture molecular interaction parameter
A_{DH}	(mol$^{-0.5}$ kg$^{0.5}$)	Debye-Hückel parameter
b_{ij}		LIQUAC middle-range interaction parameter between uncharged species i and ion j
$b_{j_\text{c}j_\text{a}}$		LIQUAC middle-range interaction parameter between cation j_c and anion j_a
b_{DH}	(mol$^{-0.5}$ kg$^{0.5}$)	Debye-Hückel parameter
b_{mix}	(m^3 kmol^{-1})	Peng-Robinson mixture volume parameter
B_{ij}	(kg kmol^{-1})	LIQUAC interaction coefficient between uncharged species i and ion j
$B_{j_\text{c}j_\text{a}}$	(kg kmol^{-1})	LIQUAC interaction coefficient between cation j_c and anion j_a
c_{ij}		LIQUAC middle-range interaction parameter between uncharged species i and ion j
$c_{j_\text{c}j_\text{a}}$		LIQUAC middle-range interaction parameter between cation j_c and anion j_a
$\underline{G}^{\text{ex}}$	(K)	Excess molar Gibbs free energy of a mixture
I_m	(mol kg^{-1})	Ionic strength of a mixture on a molal basis
m_i	(mol kg^{-1})	Molality of solute species i
m_i'	(mol kg^{-1})	Molality of solute species i calculated on an organic-free basis
M_i	(kg kmol^{-1})	Molar mass of species i
$\dot{M}_i$	(kg s^{-1})	Mass flow rate of species i
n		Number of equilibrium stages
n_i^{exp}		Number of experimental measurements for property type i
N_{anion}		Total number of anionic species
N_{cation}		Total number of cationic species
N_i	(kmol)	Number of moles of species i
N_{ion}		Total number of ionic species
N_{sol}		Total number of uncharged or solvent species
$\dot{N}_i^j$	(kmol s^{-1})	molar flow rate of species i in stream j

N_{A}	(kmol^{-1})	Avogadro constant
P	(Pa)	Pressure
q_i		Relative van der Waals surface area parameter for species i
r_i		Relative van der Waals volume parameter for species i
R	($\mathrm{J\ kmol}^{-1}\ \mathrm{K}^{-1}$)	universal gas constant
R_i		Recovery ratio of species i
T	(K)	Temperature
v_i		Volume fraction of species i
v_i'		Volume fraction of species i calculated on an salt-free basis
$\underline{V}$	($\mathrm{m}^3\ \mathrm{kmol}^{-1}$)	Molar volume of a mixture
w_i		Mass fraction of species i
w_i'		Mass fraction of species i calculated on an salt-free basis
x_i		Mole fraction of species i
x_i'		Mole fraction of species i calculated on an salt-free basis
$\boldsymbol{x}^j$		mole fraction composition vector for phase or stream j
z		Average coordination number of a molecule in the UNIQUAC excess Gibbs free energy model (fixed value of 10)
z_i		Charge number of species i
Z		Compressibility factor

Greek Letters:

γ_i		Liquid-phase activity coefficient of species i
ϵ_0	($\mathrm{F\ m}^{-1}$)	Vacuum permittivity
ϵ_i		Dielectric constant of species i
θ_i		van der Waals surface area fraction of species i
κ_i	(m^{-1})	Inverse Debye length
$\boldsymbol{\theta}_i$		LIQUAC interaction parameter vector for nonlinear regression step i
ρ_i	($\mathrm{kg\ m}^{-3}$)	Mass density of species i
ϕ_i		van der Waals volume fraction of species i
ϕ_i^{osm}		osmotic coefficient of solvent species i
$\bar{\phi}_i^j$		Fugacity coefficient of species i in phase j

Superscripts and Subscripts:

aq	Aqueous phase or aqueous stream

bin	Binary water-dimethyl ether mixture
DH	Debye-Hückel parameter
ex	Excess
exp	Value determined through experimental measurement
in	Liquid-liquid separator stream inlet
LR	Long-range
mix	Mixture properties
mod	Value determined through modeling calculations
MR	Middle-range
org	Organic phase or organic stream
osm	Osmotic coefficient
out	Liquid-liquid separator stream outlet
sol	Solvent mixture properties
SR	Short-range

Abbreviations:

DME	Dimethyl ether
ICP-OES	Inductively coupled plasma optical emission spectrometry
LLE	Liquid-liquid equilibrium
LLS	Liquid-liquid separator
MAE	Mean absolute error
MLD	Minimal-liquid discharge
PRSV	PengRobinson Stryjek-Vera
SDWE	Solvent-driven water extraction
VLE	Vapor-liquid equilibrium
VLLE	Vapor-liquid-liquid equilibrium
ZLD	Zero-liquid discharge

Appendix A. Fugacity Coefficient in the Peng-Robinson Stryjek-Vera 2 Equation of State Model

The mixture parameters a_{mix} and b_{mix} are defined in terms of the mole fractions of each species (x_i) using the van der Waals one-fluid mixing rule: $a_{\text{mix}} = \sum_i \sum_j (x_i x_j a_{ij})$ and $b_{\text{mix}} = \sum_i \sum_j (x_i x_j b_{ij})$, respectively. The averaged molecular interaction parameter a_{ij} is typically expressed in terms of a binary interaction energy (k_{ij}) between species i and j: $a_{ij} = \sqrt{a_i a_j}(1 - k_{ij})$, while the averaged molecular volume parameter b_{ij} is given by: $b_{ij} = (b_i + b_j)/2$. The fugacity coefficient for species i ($\bar{\phi}_i$) is given by [50]

$$\ln \bar{\phi}_i = \frac{1}{RT} \int_{\underline{V}\to\infty}^{\underline{V}=ZRT/P} \left[\frac{RT}{\underline{V}} - N \left(\frac{\partial P}{\partial N_i} \right)_{T,\underline{V},N_{j\neq i}} \right] d\underline{V} - \ln Z \tag{A.1}$$

Integrating Equation A.1 using the Peng-Robinson Stryjek-Vera 2 (PRSV2) equation of state (Equation 13) yields Equation 14 [50].

Appendix B. Estimating LIQUAC Excess Gibbs Free Energy Model Parameters

Figure B.7 illustrates the three steps of nonlinear regression used to calculate maximum likelihood estimators for the interaction parameters required in the LIQUAC excess Gibbs free energy model for water–DME–NaCl mixtures. In the Step 1 (purple shading), water–DME LLE, VLE, and VLLE data [80] is used to estimate H_2O–DME interaction parameters ($a^{(0)}_{H_2O\text{–DME}}$, $a^{(0)}_{\text{DME–}H_2O}$, $a^{(1)}_{H_2O\text{–DME}}$, and $a^{(1)}_{\text{DME–}H_2O}$). In the Step 2 (green shading), water-NaCl osmotic coefficient data [81, 83] is used to estimate H_2O–Na^+, H_2O–Cl^-, and Na^+–Cl^- parameters ($c_{H_2O\text{–}Na^+}$, $c_{H_2O\text{–}Cl^-}$, $b_{Na^+\text{–}Cl^-}$, and $c_{Na^+\text{–}Cl^-}$). Finally, in the Step 3, water–DME–NaCl LLE data [84] is used to estimate DME–Na^+ and DME–Cl^- parameters ($b_{H_2O\text{–}Na^+}$, $b_{H_2O\text{–}Cl^-}$, $b_{\text{DME–}Na^+}$, and $c_{\text{DME–}Cl^-}$). In the LIQUAC model, the excess Gibbs free energy of a mixture containing a single solvent species is independent of the b_{ij} parameters for solvent-ion interactions [46]. Consequently, the LIQUAC interaction parameters $b_{H_2O\text{–}Na^+}$ and $b_{H_2O\text{–}Cl^-}$ cannot be estimated from single-solvent water-NaCl osmotic coefficient data in Step 2. In this work, $b_{H_2O\text{–}Na^+}$ and $b_{H_2O\text{–}Cl^-}$ are instead estimated using mixed-solvent water–DME–NaCl LLE data. The middle-range LIQUAC excess Gibbs free energy term accounts for include ion-induced dipole, ion-dipole, and cation-anion interactions. Consequently, the middle-range LIQUAC interaction parameters between uncharged solvent species are zero ($b_{H_2O\text{–DME}} = 0$ and $c_{H_2O\text{–DME}} = 0$). Middle-range LIQUAC interaction parameters are symmetric ($b_{ji} = b_{ij}$ and $c_{ji} = c_{ij}$).

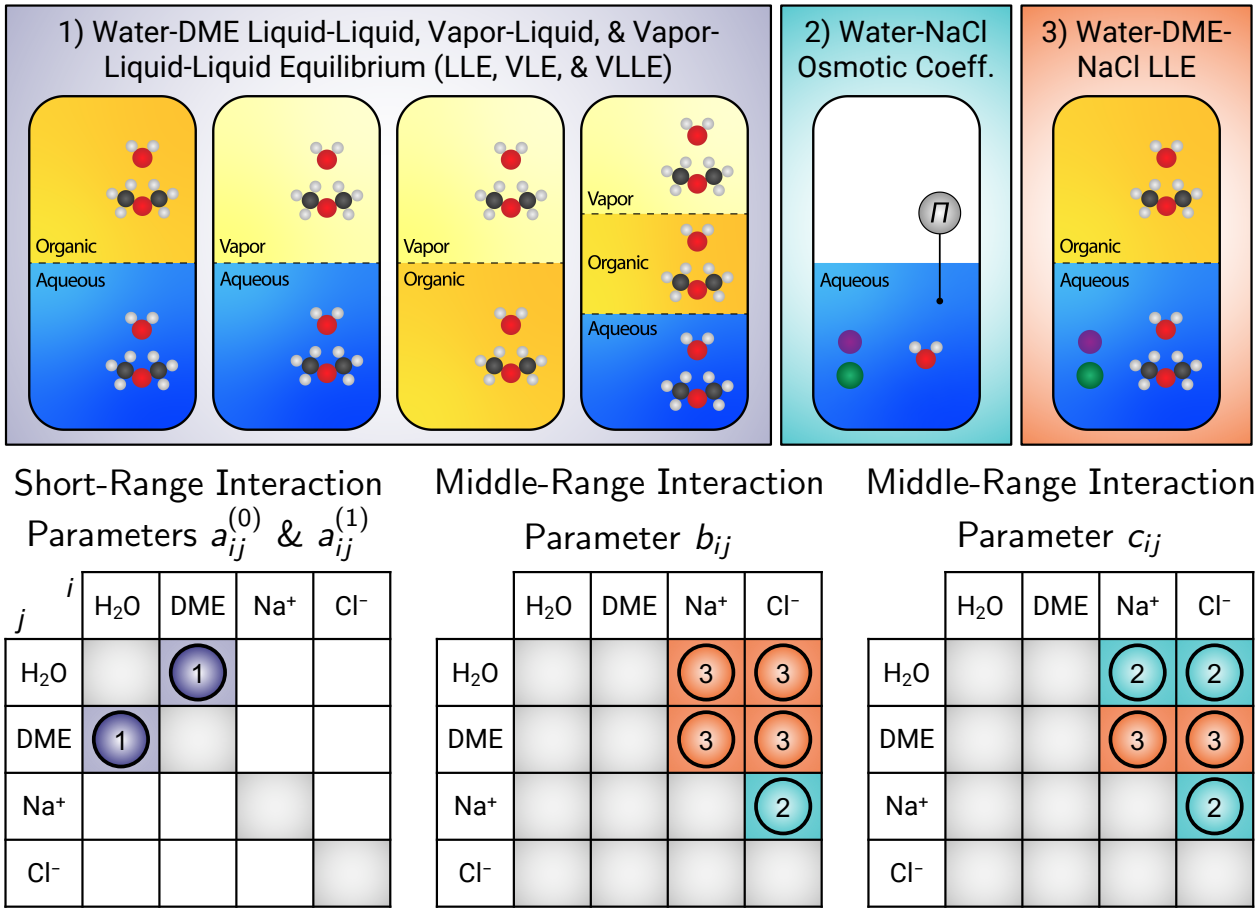

Figure B.7: Schematic diagram illustrating how the nonlinear regression of experimental fluid phase equilibrium and osmotic coefficient data is used to estimate short- ($a_{ij}^{(0)}$ and $a_{ij}^{(1)}$) and middle-range (b_{ij} and c_{ij}) interaction parameters for the LIQUAC model. Liquid-liquid, vapor-liquid, and vapor-liquid-liquid phase equilibrium (LLE, VLE, and VLLE, respectively) data for water–DME mixtures is used to estimate $a_{\mathrm{H_2O–DME}}^{(0)}$, $a_{\mathrm{DME–H_2O}}^{(0)}$, $a_{\mathrm{H_2O–DME}}^{(1)}$, and $a_{\mathrm{DME–H_2O}}^{(1)}$ (Equation 15). Osmotic coefficient data for water-NaCl mixtures is used to estimate $c_{\mathrm{H_2O–Na^+}}$, $c_{\mathrm{H_2O–Cl^-}}$, $b_{\mathrm{Na^+–Cl^-}}$, and $c_{\mathrm{Na^+–Cl^-}}$ (Equation 17). LLE data for water–DME–NaCl mixtures is used to estimate $b_{\mathrm{H_2O–Na^+}}$, $b_{\mathrm{H_2O–Cl^-}}$, $b_{\mathrm{DME–Na^+}}$, and $c_{\mathrm{DME–Cl^-}}$ (Equation 18). Middle-range LIQUAC interaction parameters are symmetric ($b_{ji} = b_{ij}$ and $c_{ji} = c_{ij}$). Short-range interaction energy parameters between solvent-ion and cation-anion pairs are set to zero to reduce overfitting [46, 48, 49].

Table B.6 shows the relative van der Waals surface area and volume parameters (r_i and q_i, respectively) used in Equation 3. For water and DME molecules, r_i and q_i are calculated using the UNIFAC group contribution method [93, 94]. For sodium and chloride ions, r_i and q_i values are taken from Mohs et al. [51].

Table B.6: Relative van der Waals surface area and volume parameters used for the combinatorial component of the UNIQUAC short-range contribution to the LIQUAC excess Gibbs free energy model (Equation 3) [51, 93, 94].

Chemical Species		Relative van der Waals Surface Area Parameter, q_i	Relative van der Waals Volume Parameter, r_i
Water	H_2O	0.9200	1.4000
DME	CH_3OCH_3	2.0461	1.9360
Sodium	Na^+	0.1518	0.2849
Chloride	Cl^-	0.9699	0.9809

Appendix C. Solubility of Sodium Chloride in the Organic Phase for Water-Dimethyl Ether-Sodium Chloride Mixtures

The solubility of NaCl in the organic phase of a water–DME-electrolyte mixture at liquid-liquid equilibrium (LLE) is negligible as a result of the very low polarity of DME, which has a dielectric constant of 5.34 at 304 K and 6.3 MPa [37]. The concentration of NaCl in water extracted using SDWE with DME ($c_{\mathrm{NaCl}}^{\mathrm{Extracted}}$) was experimentally measured for feed NaCl concentration ($c_{\mathrm{NaCl}}^{\mathrm{Feed}}$) values of approximately 70 g kg^{-1} (moderate salinity, 1.19 mol kg^{-1}) and 200 g kg^{-1} (high salinity, 3.42 mol kg^{-1}). Table C.7 shows the concentration of NaCl in the feed water, prior to mixing with DME, and in the extracted water, which is sampled from the organic phase of the water–DME–NaCl mixture at LLE. The NaCl concentration in the extracted water is measured after gradually degassing the DME-rich, organic-phase liquid sample to remove most of the DME. In each case, the concentration of NaCl in the extracted water was approximately three orders of magnitude smaller than the concentration of NaCl in the feed water: $c_{\mathrm{NaCl}}^{\mathrm{Extracted}}/c_{\mathrm{NaCl}}^{\mathrm{Feed}} \sim \mathcal{O}(10^{-3})$. At LLE, the organic phase is largely DME ($x_{\mathrm{DME}}^{\mathrm{org}} \approx 0.90$, Figure 2A). Consequently, the measured extracted water to feed water salt concentration ratio ($c_{\mathrm{NaCl}}^{\mathrm{Extracted}}/c_{\mathrm{NaCl}}^{\mathrm{Feed}}$) represents a significant overestimate of the equilibrium organic- to aqueous-phase NaCl molality ratio ($m_{\mathrm{NaCl}}^{\mathrm{org}}/m_{\mathrm{NaCl}}^{\mathrm{aq}}$). The experimental apparatus and procedure used are described in Appendix C.1 and Appendix C.2, respectively, and shown schematically in Figure C.8.

Appendix C.1. Experimental Apparatus

A single-walled glass vessel (50 mm outer diameter, 5 mm glass wall thickness, 560 mm length) with threaded ends to accommodate Teflon endcaps was used in the experiments. Endcaps were integrated with stainless-steel fittings (Swagelok) and 3.18 mm (0.125 inch) Teflon tubing to recirculate and mix the water–DME–NaCl system. Recirculation and mixing were carried out using a gear pump (Cole Parmer 115V 60 Hz console drive, EW 35215-30, equipped with a Cole Parmer micro pump head, EW-07001-40). Liquid DME was introduced

Table C.7: Sodium chloride concentration in (1) the feed water prior to contact with dimethyl ether (DME) in the solvent-driven water extraction (SDWE) test cell and (2) extracted water sampled from the organic phase at liquid-liquid equilibrium in the SDWE test cell, after the removal of DME by degassing.

	Sodium Chloride Concentration, c_{NaCl}		Salt Concentration
	Feed Water	Extracted Water	Ratio, $c_{\mathrm{NaCl}}^{\mathrm{Extracted}}/c_{\mathrm{NaCl}}^{\mathrm{Feed}}$
Moderate Salinity (7 wt.%)	66.3 g kg^{-1}	0.509 g kg^{-1}	7.7×10^{-3}
		0.458 g kg^{-1}	6.9×10^{-3}
		0.236 g kg^{-1}	3.6×10^{-3}
High Salinity (20 wt.%)	201.3 g kg^{-1}	0.237 g kg^{-1}	1.2×10^{-3}
		0.317 g kg^{-1}	1.6×10^{-3}

to the chamber via a gas cylinder with a siphon (Matheson, 99.5% purity, size 1A). Samples of the DME-rich organic phase, including the water, DME, and NaCl contained therein, were obtained using a stainless-steel sampling tube connected to a 3.18 mm (0.125 inch) ball valve (Swagelok). The opening of the sampling tube is situated at an elevated position in the vessel that is within the organic phase.

Appendix C.2. Experimental Procedure

A concentrated NaCl solution ($\approx$ 100 mL) was prepared (Nanopure H2O, 18.2 MΩ cm, Elga PURELAB flex, reagent grade NaCl, $>$ 99% purity, Sigma Aldrich) and introduced to the reaction vessel using the gear pump. Prior to use, NaCl was stored in a vacuum oven to ensure it remaining in an anhydrous state. NaCl solutions were sonicated for approximately 30 minutes to ensure all of the NaCl had dissolved. The chamber was then purged with DME five times to remove residual atmospheric gases. Liquid DME ($\approx$ 400 mL) was then added and mixed at approximately 6 bar. Mixing was accomplished by at least 15 minutes of vapor recirculation through the liquid phases via the gear pump. Samples of the organic phase were obtained via flow control at the ball valve installed in the lower endcap, capturing organic-phase water, DME, and NaCl.

Liquid samples containing the extracted water, DME, and any NaCl dissolved in the organic phase were then gradually degassed for approximately 8 hours at atmospheric pressure by loosening the caps on the collection vials. The extracted water, comprising the water that remained in the collection vials after the majority of DME had been removed by degassing, was then analyzed with inductively coupled plasma optical emission spectrometry (ICP-OES). The instrument used in analysis was an iCAP Series 6000 (Thermo Scientific), calibrated from stock solutions (1000 ppm) using a five-point calibration (0, 1, 2, 5, 10 and 20 ppm, TraceCert, Sigma Aldrich). A laboratory control standard (LCS, or sample spike) was analyzed to ensure analytical accuracy and precision. An internal standard for the ICP-

OES analysis (scandium, 4.0 mg kg^{-1}) was conducted to correct for any matrix artifacts.

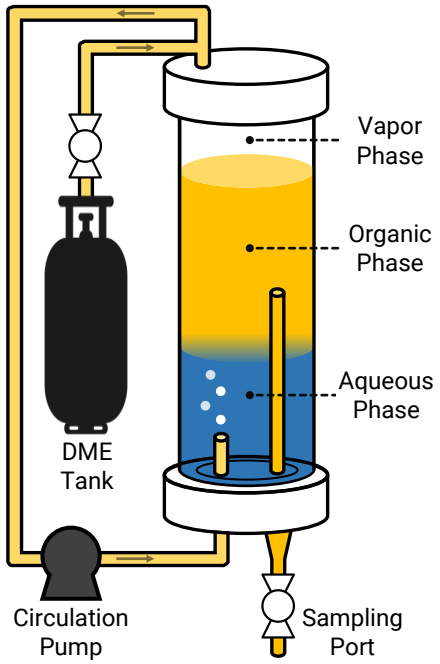

Figure C.8: Schematic diagram of the solvent-driven water extraction (SDWE) test cell used to measure the equilibrium sodium chloride (NaCl) concentration in extracted water. Saline feed water is pumped into the test chamber using a gear pump. Liquid dimethyl ether (DME) is introduced into the chamber from a gas cylinder with a siphon. A circulation pump is used to recirculate DME through the test chamber and ensure mixing. After equilibration, the organic phase, comprising extracted water, DME, and NaCl, is sampled through a sampling port using a tube that extends into the upper fluid layer.

Appendix D. Inlet Dimethyl Ether to Saline Feed Molar Flow Rate Ratio for Minimal- and Zero-Liquid Discharge Processes

Performing a mole balance on dimethyl ether (DME) entering and exiting an n-stage liquid-liquid separator (LLS, Figure 3A) gives

$$\dot{N}^{\text{org}}_{n+1} = \dot{N}^{\text{aq}}_{n} x^{\text{aq}}_{n,\text{DME}} + \dot{N}^{\text{org}}_{1} x^{\text{org}}_{1,\text{DME}} \tag{D.1}$$

where organic stream entering stage n is pure DME ($x^{\text{org}}_{n+1,\text{DME}} = 1$). The solubility of sodium chloride (NaCl) in the organic stream is assumed to be negligible and therefore the molar flow rate of sodium and chloride ions in the aqueous stream remains constant across the LLS: $\dot{N}^{\text{aq}}_{0} x^{\text{aq}}_{0,\text{Na}^+} = \dot{N}^{\text{aq}}_{n} x^{\text{aq}}_{n,\text{Na}^+}$ or $\dot{N}^{\text{aq}}_{0} x^{\text{aq}}_{0,\text{Cl}^-} = \dot{N}^{\text{aq}}_{n} x^{\text{aq}}_{n,\text{Cl}^-}$, and the organic stream contains water and DME only: $x^{\text{org}}_{a,\text{H}_2\text{O}} + x^{\text{org}}_{a,\text{DME}} = 1$. Electroneutrality in the aqueous phase leaving each stage a gives: $x^{\text{aq}}_{a,\text{Na}^+} = x^{\text{aq}}_{a,\text{Cl}^-}$ and $x^{\text{aq}}_{a,\text{H}_2\text{O}} + x^{\text{aq}}_{a,\text{DME}} + 2x^{\text{aq}}_{a,\text{Na}^+} = 1$. Furthermore, in the absence of

any chemical reactions the molar flow rate of the organic stream leaving stage 1 is given by: $\dot{N}_1^{\text{org}} = \dot{N}_0^{\text{aq}} + \dot{N}_{n+1}^{\text{org}} - \dot{N}_n^{\text{aq}}$. The mole fraction of water and DME in aqueous and organic streams at liquid-liquid equilibrium (LLE) leaving stage a can be expressed as a function of the system temperature (T) and the sodium mole fraction ($x_{a,\text{Na}^+}^{\text{aq}}$) in the aqueous stream leaving stage a

$$x_{a,\text{H}_2\text{O}}^{\text{aq}} = f_{\text{H}_2\text{O}}^{\text{LLE,aq}}\left(T, x_{a,\text{Na}^+}^{\text{aq}}\right) \qquad x_{a,\text{DME}}^{\text{aq}} = f_{\text{DME}}^{\text{LLE,aq}}\left(T, x_{a,\text{Na}^+}^{\text{aq}}\right) \tag{D.2}$$

$$x_{a,\text{H}_2\text{O}}^{\text{org}} = f_{\text{H}_2\text{O}}^{\text{LLE,org}}\left(T, x_{a,\text{Na}^+}^{\text{aq}}\right) \qquad x_{a,\text{DME}}^{\text{org}} = f_{\text{DME}}^{\text{LLE,org}}\left(T, x_{a,\text{Na}^+}^{\text{aq}}\right) \tag{D.3}$$

Rearranging Equation D.1 gives

$$\frac{\dot{N}_{n+1}^{\text{org}}}{\dot{N}_0^{\text{aq}}} = \left(\frac{\dot{N}_n^{\text{aq}}}{\dot{N}_0^{\text{aq}}}\right) x_{n,\text{DME}}^{\text{aq}} + \left(1 + \frac{\dot{N}_{n+1}^{\text{org}}}{\dot{N}_0^{\text{aq}}} - \frac{\dot{N}_n^{\text{aq}}}{\dot{N}_0^{\text{aq}}}\right) x_{1,\text{DME}}^{\text{org}} \tag{D.4}$$

$$\frac{\dot{N}_{n+1}^{\text{org}}}{\dot{N}_0^{\text{aq}}} = \frac{1}{x_{1,\text{H}_2\text{O}}^{\text{org}}} - 1 - \left(\frac{x_{1,\text{DME}}^{\text{org}} - x_{n,\text{DME}}^{\text{aq}}}{x_{1,\text{H}_2\text{O}}^{\text{org}}}\right)\left(\frac{x_{0,\text{Na}^+}^{\text{aq}}}{x_{n,\text{Na}^+}^{\text{aq}}}\right) \tag{D.5}$$

In the limiting case as $x_{0,\text{Na}^+}^{\text{aq}}/x_{n,\text{Na}^+}^{\text{aq}} \to 1$

$$\frac{\dot{N}_{n+1}^{\text{org}}}{\dot{N}_0^{\text{aq}}} \to \frac{x_{1,\text{DME}}^{\text{aq}}}{x_{1,\text{H}_2\text{O}}^{\text{org}}} \tag{D.6}$$

The aqueous-phase DME mole fraction at LLE ranges from approximately 0.03 to 0.16 at 300 K (Figure 2B), while the organic-phase water mole fraction at LLE ranges from approximately 0.09 to 0.16 (Figure 2A) at the same temperature.

In the limiting case as $\dot{N}_{n+1}^{\text{org}}/\dot{N}_0^{\text{aq}} \to 0$

$$\frac{x_{0,\text{Na}^+}^{\text{aq}}}{x_{n,\text{Na}^+}^{\text{aq}}} \to \frac{1}{1 - \dfrac{x_{1,\text{DME}}^{\text{aq}}}{x_{1,\text{DME}}^{\text{org}}}} \tag{D.7}$$

The organic-phase DME mole fraction at LLE ranges from approximately 0.84 to 0.91 at 300 K (Figure 2B).

Appendix D.1. Dimethyl Ether Required for a One-Stage Liquid-Liquid Separator

For a one-stage LLS, the inlet DME to saline feed molar flow rate ratio ($\dot{N}_2^{\text{org}}/\dot{N}_0^{\text{aq}}$ in the leaving streams labeling notation) is given by:

$$\frac{\dot{N}_2^{\text{org}}}{\dot{N}_0^{\text{aq}}} = \frac{1}{x_{1,\text{H}_2\text{O}}^{\text{org}}} - 1 - \left(\frac{x_{1,\text{DME}}^{\text{org}} - x_{1,\text{DME}}^{\text{aq}}}{x_{1,\text{H}_2\text{O}}^{\text{org}}}\right)\left(\frac{x_{0,\text{Na}^+}^{\text{aq}}}{x_{1,\text{Na}^+}^{\text{aq}}}\right) \tag{D.8}$$

For a specified organic-free concentrated brine molality ($m_{\text{NaCl}}^{\prime\,\text{aq,out}}$) and system temperature (T), the outlet sodium mole fraction ($x_{1,\text{Na}^+}^{\text{aq}}$) is fixed. Consequently, the equilibrium values $x_{1,\text{H}_2\text{O}}^{\text{org}} = f_{\text{H}_2\text{O}}^{\text{LLE,org}}\left(T, x_{1,\text{Na}^+}^{\text{aq}}\right)$, $x_{1,\text{DME}}^{\text{aq}} = f_{\text{DME}}^{\text{LLE,aq}}\left(T, x_{1,\text{Na}^+}^{\text{aq}}\right)$, and $x_{1,\text{DME}}^{\text{org}} = f_{\text{DME}}^{\text{LLE,org}}\left(T, x_{1,\text{Na}^+}^{\text{aq}}\right)$ are fixed and $\dot{N}_2^{\text{org}}/\dot{N}_0^{\text{aq}}$ decreases linearly with $x_{0,\text{Na}^+}^{\text{aq}}$. The inlet DME to saline feed molar flow rate ratio can be written as

$$\frac{\dot{N}_2^{\text{org}}}{\dot{N}_0^{\text{aq}}} = K_1\left(1 - \frac{x_{\text{Na}^+}^{\text{aq,in}}}{K_2}\right) \tag{D.9}$$

where K_1 and K_2 are constants at a specified $m_{\text{NaCl}}^{\prime\,\text{aq,out}}$ and T. The constant K_2 is slightly larger than the outlet sodium mole fraction: $K_2 = x_{1,\text{Na}^+}^{\text{aq}}/[1 - (x_{1,\text{DME}}^{\text{aq}}/x_{1,\text{DME}}^{\text{org}})]$.

The saline feed stream contains water and NaCl only, and thus the inlet sodium mole fraction ($x_{0,\text{Na}^+}^{\text{aq}}$) can be expressed in terms of inlet saline feed molality ($m_{0,\text{NaCl}}^{\text{aq}}$)

$$x_{0,\text{Na}^+}^{\text{aq}} = \frac{m_{0,\text{NaCl}}^{\text{aq}}}{\dfrac{1}{M_{\text{H}_2\text{O}}} + 2m_{0,\text{NaCl}}^{\text{aq}}} \tag{D.10}$$

Appendix D.2. Dimethyl Ether Required for a Multistage Liquid-Liquid Separator

For a multistage LLS ($n \geqslant 2$), the inlet DME to saline feed molar flow rate ratio ($\dot{N}_{n+1}^{\text{org}}/\dot{N}_0^{\text{aq}}$ in the leaving streams labeling notation) is given by

$$\frac{\dot{N}_{n+1}^{\text{org}}}{\dot{N}_0^{\text{aq}}} = \frac{1}{x_{1,\text{H}_2\text{O}}^{\text{org}}} - 1 - \left(\frac{x_{1,\text{DME}}^{\text{org}} - x_{n,\text{DME}}^{\text{aq}}}{x_{1,\text{H}_2\text{O}}^{\text{org}}}\right)\left(\frac{x_{0,\text{Na}^+}^{\text{aq}}}{x_{n,\text{Na}^+}^{\text{aq}}}\right) \tag{D.11}$$

In the limiting case as ($x_{0,\text{Na}^+}^{\text{aq}} \to 0$):

$$\frac{\dot{N}_{n+1}^{\text{org}}}{\dot{N}_0^{\text{aq}}} \to \frac{1}{x_{1,\text{H}_2\text{O}}^{\text{org}}} - 1 \tag{D.12}$$

The water mole fraction in the outflowing organic stream is a function of system temperature and the sodium mole fraction in the aqeuoys stream leaving the first stage $x_{1,\text{H}_2\text{O}}^{\text{org}} =$

$f_{H_2O}^{LLE,org}\left(T, x_{1,Na^+}^{aq}\right)$. In an n-stage LLS, the majority of the water transfer occurs in the n^{th} or last stage (Figure 3B) and thus $x_{1,Na^+}^{aq} \to 0$ as $x_{0,Na^+}^{aq} \to 0$. As x_{0,Na^+}^{aq} is reduced to the inlet DME to saline feed molar flow rate ratio approaches the binary water–DME mixture limit

$$\lim_{x_{1,Na^+}^{aq} \to 0} \left(\frac{\dot{N}_{n+1}^{org}}{\dot{N}_0^{aq}} \right) = \frac{1}{x_{H_2O}^{org,bin}(T)} - 1 \tag{D.13}$$

where $x_{H_2O}^{org,bin}(T) = x_{H_2O}^{org}\left(T, x_{Na^+}^{aq} = 0\right)$ is the organic-phase water mole fraction at LLE in a binary water–DME mixture as a function of temperature (left-hand side $x_{NaCl}^{aq} = 0$ curve in Figure 2A). In this scenario, the limiting value of $\dot{N}_{n+1}^{org}/\dot{N}_0^{aq}$ is independent of n and x_{n,Na^+}^{aq} and, therefore, independent of $m_{0,NaCl}^{\prime aq,out}$ (two-stage curves in Figure 5).

Appendix E. Dimethyl Ether Recovery Ratio

Figure E.9 shows the DME recovery ratio ratio ($R_{DME} = \dot{N}_{DME}^{org,out}/\dot{N}_{DME}^{org,in}$) as a function of feed molality ($m_{NaCl}^{aq,in}$) and the inlet DME to saline feed molar flow rate ratio ($\dot{N}_{DME}^{org,in}/\dot{N}_{Feed}^{aq,in}$) for SDWE with a one-stage LLS without any additional solvent recovery steps. System temperature is fixed at 300 K throughout. Contour lines indicating R_{DME} values of 0.95, 0.96, 0.97, 0.98, and 0.99 are shown. The rapid salting out of DME from the aqueous phase at LLE (Figure 2B) yields high DME recovery ratios, particularly when the outlet concentrated brine molality is high (Figure 6A).

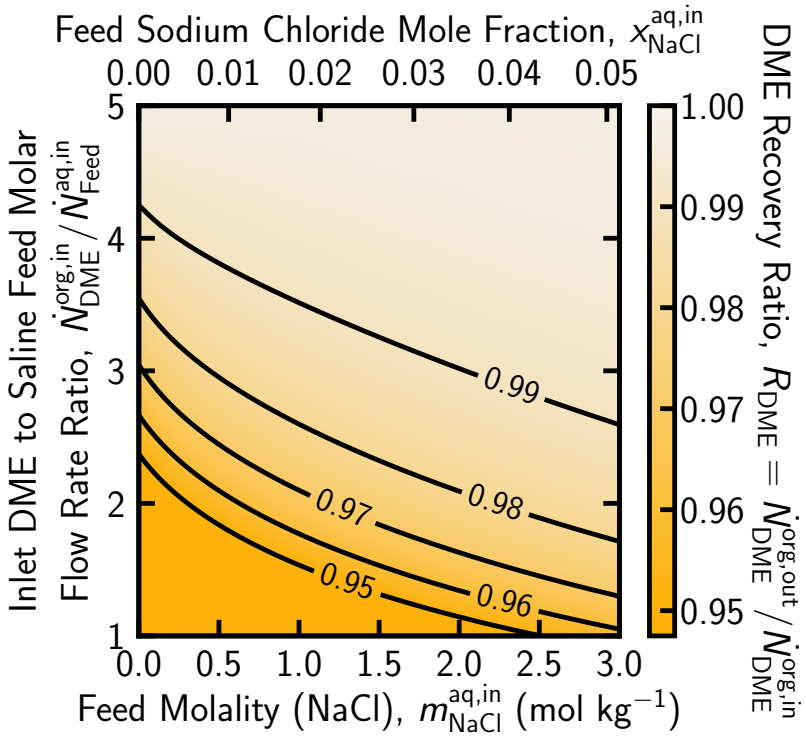

Figure E.9: Dimethyl ether (DME) recovery ratio ($R_{\mathrm{DME}} = \dot{N}_{\mathrm{DME}}^{\mathrm{org,out}}/\dot{N}_{\mathrm{DME}}^{\mathrm{org,in}}$) as a function of feed molality ($m_{\mathrm{NaCl}}^{\mathrm{aq,in}}$) and inlet DME to saline feed molar flow rate ratio ($\dot{N}_{\mathrm{DME}}^{\mathrm{org,in}}/\dot{N}_{\mathrm{Feed}}^{\mathrm{aq,in}}$) for one-stage solvent-driven water extraction (SDWE). The feed sodium chloride mole fraction is given by: $x_{\mathrm{NaCl}}^{\mathrm{aq,in}} = m_{\mathrm{NaCl}}^{\mathrm{aq,in}}/\left[\left(1/M_{\mathrm{H_2O}}\right) + m_{\mathrm{NaCl}}^{\mathrm{aq,in}}\right]$. System temperature is fixed at 300 K throughout. Calculations are performed treating Na^+ and Cl^- as separate species.

References

[1] T. Tong, M. Elimelech, The Global Rise of Zero Liquid Discharge for Wastewater Management: Drivers, Technologies, and Future Directions, Environmental Science and Technology 50 (13) (2016) 6846–6855. doi:10.1021/acs.est.6b01000.

[2] G. P. Thiel, E. W. Tow, L. D. Banchik, H. W. Chung, J. H. Lienhard, Energy consumption in desalinating produced water from shale oil and gas extraction, Desalination 366 (2015) 94–112. doi:10.1016/j.desal.2014.12.038.

[3] C. E. Clark, R. M. Horner, C. B. Harto, Life cycle water consumption for shale gas and conventional natural gas, Environmental Science and Technology 47 (20) (2013) 11829–11836. doi:10.1021/es4013855.

[4] K. Hoelzer, A. J. Sumner, O. Karatum, R. K. Nelson, B. D. Drollette, M. P. O'Connor, E. L. D'Ambro, G. J. Getzinger, P. L. Ferguson, C. M. Reddy, M. Elsner, D. L. Plata, Indications of Transformation Products from Hydraulic Fracturing Additives in Shale-Gas Wastewater, Environmental Science and Technology 50 (15) (2016) 8036–8048. doi:10.1021/acs.est.6b00430.

[5] S. B. Grant, J. D. Saphores, D. L. Feldman, A. J. Hamilton, T. D. Fletcher, P. L. Cook, M. Stewardson, B. F. Sanders, L. A. Levin, R. F. Ambrose, A. Deletic, R. Brown, S. C. Jiang, D. Rosso, W. J. Cooper, I. Marusic, Taking the "waste" out of "wastewater" for human water security and ecosystem sustainability, Science 337 (6095) (2012) 681–686. doi:10.1126/science.1216852.

[6] D. L. Shaffer, L. H. Arias Chavez, M. Ben-Sasson, S. Romero-Vargas Castrillón, N. Y. Yip, M. Elimelech, Desalination and reuse of high-salinity shale gas produced water: Drivers, technologies, and future directions, Environmental Science and Technology 47 (17) (2013) 9569–9583. doi:10.1021/es401966e.

[7] T. A. Larsen, S. Hoffmann, C. Lüthi, B. Truffer, M. Maurer, Emerging solutions to the water challenges of an urbanizing world, Science 352 (6288) (2016) 928–933. doi:10.1126/science.aad8641.

[8] V. R. Moreira, Y. A. R. Lebron, M. C. S. Amaral, Mining from wastewater: Perspectives and current practices of non-dispersive solvent extraction for metallic compounds valorization, Chemical Engineering Journal 425 (2021) 130711. doi:10.1016/j.cej.2021.130711.

[9] C. W. Noack, D. A. Dzombak, A. K. Karamalidis, Determination of Rare Earth Elements in Hypersaline Solutions Using Low-Volume, Liquid-Liquid Extraction, Environmental Science and Technology 49 (16) (2015) 9423–9430. doi:10.1021/acs.est.5b00151.

[10] B. K. Pramanik, L. D. Nghiem, F. I. Hai, Extraction of strategically important elements from brines: Constraints and opportunities, Water Research 168 (2020) 115149. doi:10.1016/j.watres.2019.115149.

[11] C. F. Baspineiro, J. Franco, V. Flexer, Potential water recovery during lithium mining from high salinity brines, Science of the Total Environment 720 (2020) 137523. doi:10.1016/j.scitotenv.2020.137523.

[12] F. Xie, T. A. Zhang, D. Dreisinger, F. Doyle, A critical review on solvent extraction of rare earths from aqueous solutions, Minerals Engineering 56 (2014) 10–28. doi:10.1016/j.mineng.2013.10.021.

[13] V. Flexer, C. F. Baspineiro, C. I. Galli, Lithium recovery from brines: A vital raw material for green energies with a potential environmental impact in its mining and processing (oct 2018). doi:10.1016/j.scitotenv.2018.05.223.

[14] S. Wu, L. Wang, L. Zhao, P. Zhang, H. El-Shall, B. Moudgil, X. Huang, L. Zhang, Recovery of rare earth elements from phosphate rock by hydrometallurgical processes A critical review, Chemical Engineering Journal 335 (August 2017) (2018) 774–800. doi:10.1016/j.cej.2017.10.143.

[15] M. E. Leblebici, S. Kuhn, G. D. Stefanidis, T. Van Gerven, Milli-channel mixer and phase separator for solvent extraction of rare earth elements, Chemical Engineering Journal 293 (2016) 273–280. doi:10.1016/j.cej.2016.02.083.

[16] A. Kumar, Y. Kim, X. Su, H. Fukuda, G. Naidu, F. Du, S. Vigneswaran, E. Drioli, T. A. Hatton, J. H. Lienhard, Advances and challenges in metal ion separation from water, Trends in Chemistry 3 (10) (2021) 819–831. doi:10.1016/j.trechm.2021.08.001.

[17] Z. Amjad, P. G. Koutsoukos, Mineral Scales and Deposits: Scientific and Technological Approaches, 1st Edition, Elsevier, Amsterdam, Netherlands, 2015. doi:10.1201/9781420071450.

[18] T. Tong, S. Zhao, C. Boo, S. M. Hashmi, M. Elimelech, Relating Silica Scaling in Reverse Osmosis to Membrane Surface Properties, Environmental Science and Technology 51 (8) (2017) 4396–4406. doi:10.1021/acs.est.6b06411.

[19] G. U. Semblante, J. Z. Lee, L. Y. Lee, S. L. Ong, H. Y. Ng, Brine pre-treatment technologies for zero liquid discharge systems, Desalination 441 (January) (2018) 96–111. doi:10.1016/j.desal.2018.04.006.

[20] A. Panagopoulos, K. J. Haralambous, Minimal Liquid Discharge (MLD) and Zero Liquid Discharge (ZLD) strategies for wastewater management and resource recovery-Analysis, challenges and prospects, Journal of Environmental Chemical Engineering 8 (5) (2020) 104418. doi:10.1016/j.jece.2020.104418.

[21] R. R. Davison, W. H. Smith, D. W. Hood, Structure and Amine-Water Solubility in Desalination by Solvent Extraction, Journal of Chemical and Engineering Data 5 (4) (1960) 420–423. doi:10.1021/je60008a005.

[22] R. R. Davison, W. B. Harris, W. H. Smith, A solvent extraction desalination pilot plant, Desalination 3 (1) (1967) 17–26.

[23] L. Lazare, The Puraq seawater desalination process, Desalination 42 (1) (1982) 11–16. doi:10.1016/0011-9164(92)80016-3.

[24] L. Lazare, The Puraq seawater desalination process - An update, Desalination 85 (3) (1992) 345–360. doi:10.1016/0011-9164(92)80016-3.

[25] A. Bajpayee, T. Luo, A. Muto, G. Chen, Very low temperature membrane-free desalination by directional solvent extraction, Energy & Environmental Science 4 (5) (2011) 1672. doi:10.1039/c1ee01027a.

[26] T. Luo, A. Bajpayee, G. Chen, Directional solvent for membrane-free water desalination-A molecular level study, Journal of Applied Physics 110 (054905) (2011) 1–6. doi:10.1063/1.3627239.

[27] A. Bajpayee, D. Kraemer, A. J. Muto, G. Chen, J. H. Lienhard, B. B. Mikic, Water desalination using directional solvent extraction, US Patent #8119007, 21 February 2012.

[28] A. Bajpayee, D. Kraemer, A. J. Muto, G. Chen, J. H. Lienhard, B. B. Mikic, Water desalination using directional solvent extraction, US Patent #8501007, 6 August 2013.

[29] A. Bajpayee, Directional Solvent Extraction Desalination, Ph.D. thesis, Massachusetts Institute of Technology, Cambridge, MA (2012).

[30] C. Boo, R. K. Winton, K. M. Conway, N. Y. Yip, Membrane-less and Non-Evaporative Desalination of Hypersaline Brines by Temperature Swing Solvent Extraction, Environmental Science and Technology Letters 6 (6) (2019) 359–364. doi:10.1021/acs.estlett.9b00182.

[31] C. Boo, I. H. Billinge, X. Chen, K. M. Shah, N. Y. Yip, Zero Liquid Discharge of Ultrahigh-Salinity Brines with Temperature Swing Solvent Extraction, Environmental Science and Technology 54 (14) (2020) 9124–9131. doi:10.1021/acs.est.0c02555.

[32] C. Boo, H. Qi, I. H. Billinge, K. M. Shah, H. Fan, N. Y. Yip, Thermomorphic Hydrophilicity Base-Induced Precipitation for Effective Descaling of Hypersaline Brines, ACS ES&T Engineering 1 (9) (2021) 1351–1359. doi:10.1021/acsestengg.1c00160.

[33] Z. B. Alfassi, L. Ata, Separation of the System NaCI-NaBr-Nal by Solventing Out from Aqueous Solution, Separation Science and Technology 18 (7) (1983) 593–601. doi:10.1080/01496398308060298.

[34] C. Boo, M. Elimelech, Thermal desalination membranes: Carbon nanotubes keep up the heat, Nature Nanotechnology 12 (6) (2017) 501–503. doi:10.1038/nnano.2017.114.

[35] D. B. Sanap, K. D. Kadam, M. Narayan, S. Kasthurirangan, P. R. Nemade, V. H. Dalvi, Analysis of saline water desalination by directed solvent extraction using octanoic acid, Desalination 357 (2015) 150–162. doi:10.1016/j.desal.2014.11.020.

[36] S. Alotaibi, O. M. Ibrahim, S. Luo, T. Luo, Modeling of a continuous water desalination process using directional solvent extraction, Desalination 420 (July) (2017) 114–124. doi:10.1016/j.desal.2017.07.004.

[37] W. Eltringham, O. J. Catchpole, Relative permittivity measurements of gaseous, liquid, and supercritical dimethyl ether, Journal of Chemical and Engineering Data 52 (2) (2007) 363–367. doi:10.1021/je060283w.

[38] J. Wu, Y. Zhou, E. W. Lemmon, An Equation of State for the Thermodynamic Properties of Dimethyl Ether, Journal of Physical and Chemical Reference Data 40 (2) (2011) 023104. doi:10.1063/1.3582533.

[39] D. S. Abrams, J. M. Prausnitz, Statistical thermodynamics of liquid mixtures: A new expression for the excess Gibbs energy of partly or completely miscible systems, AIChE Journal 21 (1) (1975) 116–128. doi:10.1002/aic.690210115.

[40] J. Li, H.-M. Polka, J. Gmehling, A gE model for single and mixed solvent electrolyte systems: 1. Model and results for strong electrolytes, Fluid Phase Equilibria 94 (1994) 89–114. doi:10.1016/0378-3812(94)87052-7.

[41] H.-M. Polka, J. Li, J. Gmehling, A gE model for single and mixed solvent electrolyte systems: 2. Results and comparison with other models, Fluid Phase Equilibria 94 (1994) 115–127. doi:10.1016/0378-3812(94)87053-5.

[42] M.-Y. Li, L.-S. Wang, B. Jiang, J. Gmehling, Generalized LIQUAC model for the single- and mixed-solvent strong electrolyte systems, AIChE Journal 57 (9) (2011) 2535–2546. doi:10.1002/aic.12445.

[43] M. Y. Li, L. S. Wang, J. Gmehling, Thermodynamics of phase equilibria in aqueous strong electrolyte systems, Industrial and Engineering Chemistry Research 50 (6) (2011) 3621–3631. doi:10.1021/ie101428j.

[44] T. F. Anderson, J. M. Prausnitz, Application of the UNIQUAC Equation to Calculation of Multicomponent Phase Equilibria. 1. Vapor-Liquid Equilibria, Industrial and Engineering Chemistry Process Design and Development 17 (4) (1978) 552–561. doi:10.1021/i260068a028.

[45] T. F. Anderson, J. M. Prausnitz, Application of the UNIQUAC equation to calculation of multicomponent phase equilibria. 2. Liquid-liquid equilibria, Industrial and Engineering Chemistry Process Design and Development 17 (4) (1978) 561–567. doi:10.1021/i260068a029.

[46] W. Yan, M. Topphoff, C. Rose, J. Gmehling, Prediction of vapor-liquid equilibria in mixed-solvent electrolyte systems using the group contribution concept, Fluid Phase Equilibria 162 (1-2) (1999) 97–113. doi:10.1016/S0378-3812(99)00201-0.

[47] S.-T. Lin, S. I. Sandler, A Priori Phase Equilibrium Prediction from a Segment Contribution Solvation Model, Industrial and Engineering Chemistry Research 41 (2002) 899–913. doi:10.1021/ie001047w.

[48] J. Kiepe, O. Noll, J. Gmehling, Modified LIQUAC and modified LIFAC - A further development of electrolyte models for the reliable prediction of phase equilibria with strong electrolytes, Industrial and Engineering Chemistry Research 45 (7) (2006) 2361–2373. doi:10.1021/ie0510122.

[49] A. Zuend, C. Marcolli, B. P. Luo, T. Peter, A thermodynamic model of mixed organic-inorganic aerosols to predict activity coefficients, Atmospheric Chemistry and Physics 8 (16) (2008) 4559–4593. doi:10.5194/acp-8-4559-2008.

[50] S. I. Sandler, Chemical, Biochemical, and Engineering Thermodynamics, 5th Edition, John Wiley & Sons, New York, 2017.

[51] A. Mohs, J. Gmehling, A revised LIQUAC and LIFAC model (LIQUAC*/LIFAC*) for the prediction of properties of electrolyte containing solutions, Fluid Phase Equilibria 337 (2013) 311–322. doi:10.1016/J.FLUID.2012.09.023.

[52] R. H. Fowler, E. A. Guggenheim, Statistical Thermodynamics: A Version of Statistical Mechanics for Students of Physics and Chemistry, 2nd Edition, Cambridge University Press, Cambridge, UK, 1949.

[53] M. J. D. M. Cardoso, J. P. O'Connell, Activity coefficients in mixed solvent electrolyte solutions, Fluid Phase Equilibria 33 (3) (1987) 315–326. doi:10.1016/0378-3812(87)85043-4.

[54] J. Li, Y. Lin, J. Gmehling, gE model for single- and mixed-solvent electrolyte systems. 3. Prediction of salt solubilities in aqueous electrolyte systems, Industrial and Engineering Chemistry Research 44 (5) (2005) 1602–1609. doi:10.1021/ie049283k.

[55] K. Thomsen, P. Rasmussen, R. Gani, Correlation and prediction of thermal properties and phase behaviour for a class of aqueous electrolyte systems, Chemical Engineering Science 51 (14) (1996) 3675–3683. doi:10.1016/0009-2509(95)00418-1.

[56] M. C. Iliuta, K. Thomsen, P. Rasmussen, Extended UNIQUAC model for correlation and prediction of vapourliquidsolid equilibria in aqueous salt systems containing non-electrolytes. Part A. Methanolwatersalt systems, Chemical Engineering Science 55 (14) (2000) 2673–2686. doi:10.1016/S0009-2509(99)00534-5.

[57] B. Zhuang, G. Ramanauskaite, Z. Y. Koa, Z. G. Wang, Like dissolves like: A first-principles theory for predicting liquid miscibility and mixture dielectric constant, Science Advances 7 (7) (2021) 7275–7287. doi:10.1126/sciadv.abe7275.

[58] B. Sander, A. Fredenslund, P. Rasmussen, Calculation of vapour-liquid equilibria in mixed solvent/salt systems using an extended UNIQUAC equation, Chemical Engineering Science 41 (5) (1986) 1171–1183. doi:10.1016/0009-2509(86)87090-7.

[59] E. A. Macedo, P. Skovborg, P. Rasmussen, Calculation of phase equilibria for solutions of strong electrolytes in solventwater mixtures, Chemical Engineering Science 45 (4) (1990) 875–882. doi:10.1016/0009-2509(90)85009-3.

[60] D. Y. Peng, D. B. Robinson, A New Two-Constant Equation of State, Industrial and Engineering Chemistry Fundamentals 15 (1) (1976) 59–64. doi:10.1021/i160057a011.

[61] R. Stryjek, J. H. Vera, PRSV: An improved PengRobinson equation of state for pure compounds and mixtures, The Canadian Journal of Chemical Engineering 64 (2) (1986) 323–333. doi:10.1002/cjce.5450640224.

[62] R. Stryjek, J. H. Vera, PRSV An improved PengRobinson equation of state with new mixing rules for strongly nonideal mixtures, The Canadian Journal of Chemical Engineering 64 (2) (1986) 334–340. doi:10.1002/cjce.5450670328.

[63] R. Stryjek, J. H. Vera, PRSV2: A cubic equation of state for accurate vapor-liquid equilibria calculations, The Canadian Journal of Chemical Engineering 64 (5) (1986) 820–826. doi:10.1002/cjce.5450640516.

[64] P. Proust, J. H. Vera, PRSV: The Stryjek-Vera modification of the Peng-Robinson equation of state. Parameters for other pure compounds of industrial interest, The Canadian Journal of Chemical Engineering 67 (1) (1989) 170–173. doi:https://doi.org/10.1002/cjce.5450670125.

[65] P. M. Mathias, H. C. Klotz, J. M. Prausnitz, Equation-of-State mixing rules for multicomponent mixtures: the problem of invariance, Fluid Phase Equilibria 67 (C) (1991) 31–44. doi:10.1016/0378-3812(91)90045-9.

[66] H. Orbey, S. I. Sandler, On the combination of equation of state and excess free energy models, Fluid Phase Equilibria 111 (1) (1995) 53–70. doi:10.1016/0378-3812(95)02764-6.

[67] R. Stryjek, J. H. Vera, An Improved Cubic Equation of State, in: Equations of State, Vol. 300 of ACS Symposium Series, American Chemical Society, 1986, pp. 27–560. doi:doi:10.1021/bk-1986-0300.ch027.

[68] U. Weidlich, J. Gmehling, A Modified UNIFAC Model. 1. Prediction of VLE, hE, and γ, Industrial and Engineering Chemistry Research 26 (7) (1987) 1372–1381. doi:10.1021/ie00067a018.

[69] C. C. Chen, C. P. Bokis, P. M. Mathias, Segment-based excess Gibbs energy model for aqueous organic electrolytes, AIChE Journal 47 (11) (2001) 2593–2602. doi:10.1002/aic.690471122.

[70] Y. Song, C. C. Chen, Symmetric nonrandom two-liquid segment activity coefficient model for electrolytes, Industrial and Engineering Chemistry Research 48 (11) (2009) 5522–5529. doi:10.1021/ie900006g.

[71] A. Klamt, Conductor-like screening model for real solvents: A new approach to the quantitative calculation of solvation phenomena, Journal of Physical Chemistry 99 (7) (1995) 2224–2235. doi:10.1021/j100007a062.

[72] S. Wang, Y. Song, C. C. Chen, Extension of COSMO-SAC solvation model for electrolytes, Industrial and Engineering Chemistry Research 50 (1) (2011) 176–187. doi:10.1021/ie100689g.

[73] M.-T. Hsieh, S. T. Lin, A predictive model for the excess gibbs free energy of fully dissociated electrolyte solutions, AIChE Journal 57 (4) (2011) 1061–1074. doi:10.1002/aic.12325.

[74] T. Ingram, T. Gerlach, T. Mehling, I. Smirnova, Extension of COSMO-RS for monoatomic electrolytes: Modeling of liquid-liquid equilibria in presence of salts, Fluid Phase Equilibria 314 (2012) 29–37. doi:10.1016/j.fluid.2011.09.021.

[75] I. H. Bell, E. Mickoleit, C. M. Hsieh, S. T. Lin, J. Vrabec, C. Breitkopf, A. Jäger, A Benchmark Open-Source Implementation of COSMO-SAC, Journal of Chemical Theory and Computation 16 (4) (2020) 2635–2646. doi:10.1021/acs.jctc.9b01016.

[76] Y. Chung, R. J. Gillis, W. H. Green, Temperature-dependent vaporliquid equilibria and solvation free energy estimation from minimal data, AIChE Journal 66 (2020) e16976. doi:10.1002/aic.16976.

[77] F. H. Vermeire, W. H. Green, Transfer learning for solvation free energies: From quantum chemistry to experiments, Chemical Engineering Journal 418 (March) (2021) 129307. doi:10.1016/j.cej.2021.129307.

[78] P. Sappidi, G. Barbosa, B. D. Rabideau, S. T. Weinman, C. H. Turner, Molecular Simulation of High-Salinity Brines in Contact with Diisopropylamine and Tripropylamine Solvents, Industrial and Engineering Chemistry Research 60 (21) (2021) 7917–7925. doi:10.1021/acs.iecr.1c01057.

[79] G. D. Barbosa, J. E. Bara, S. T. Weinman, C. H. Turner, Molecular aspects of temperature swing solvent extraction for brine desalination using imidazole-based solvents, Chemical Engineering Science 247 (2022) 116866. doi:10.1016/j.ces.2021.116866.

[80] H. Holldorff, H. Knapp, Vapor pressures of n-butane, dimethyl ether, methyl chloride, methanol and the vapor-liquid equilibrium of dimethyl ether - methanol: Experimental apparatus, results and data reduction, Fluid Phase Equilibria 40 (1-2) (1988) 113–125. doi:10.1016/0378-3812(88)80024-4.

[81] R. A. Robinson, R. H. Stokes, Electrolyte Solutions, Dover Publications, Mineola, NY, 2002.

[82] A. D. Wilson, Idaho Database of Solution Thermodynamics (2021).

[83] B. P. Feeley, M. A. Overton, M. M. Galloway, T. J. Lecrivain, A. D. Wilson, Idaho database of solution thermodynamics, Journal of Molecular Liquids 338 (2021) 116574. doi:10.1016/j.molliq.2021.116574.

[84] J. S. McNally, Z. H. Foo, A. Deshmukh, C. J. Orme, J. H. Lienhard, A. D. Wilson, Solute displacement in the aqueous phase of waterNaClorganic ternary mixtures relevant to solvent-driven water treatment, RSC Advances 10 (49) (2020) 29516–29527. doi:10.1039/D0RA06361D.

[85] P. Virtanen, R. Gommers, T. E. Oliphant, M. Haberland, T. Reddy, D. Cournapeau, E. Burovski, P. Peterson, W. Weckesser, J. Bright, S. J. van der Walt, M. Brett, J. Wilson, K. J. Millman, N. Mayorov, A. R. Nelson, E. Jones, R. Kern, E. Larson, C. J. Carey, I. Polat, Y. Feng, E. W. Moore, J. VanderPlas, D. Laxalde, J. Perktold, R. Cimrman, I. Henriksen, E. A. Quintero, C. R. Harris, A. M. Archibald, A. H. Ribeiro, F. Pedregosa, P. van Mulbregt, A. Vijaykumar, A. P. Bardelli, A. Rothberg, A. Hilboll, A. Kloeckner, A. Scopatz, A. Lee, A. Rokem, C. N. Woods, C. Fulton, C. Masson, C. Häggström, C. Fitzgerald, D. A. Nicholson, D. R. Hagen, D. V. Pasechnik, E. Olivetti, E. Martin, E. Wieser, F. Silva, F. Lenders, F. Wilhelm, G. Young, G. A. Price, G. L. Ingold, G. E. Allen, G. R. Lee, H. Audren, I. Probst, J. P. Dietrich, J. Silterra, J. T. Webber, J. Slavič, J. Nothman, J. Buchner, J. Kulick, J. L. Schönberger, J. V. de Miranda Cardoso, J. Reimer, J. Harrington, J. L. C. Rodríguez, J. Nunez-Iglesias, J. Kuczynski, K. Tritz, M. Thoma, M. Newville, M. Kümmerer, M. Bolingbroke, M. Tartre, M. Pak, N. J. Smith, N. Nowaczyk, N. Shebanov, O. Pavlyk, P. A. Brodtkorb, P. Lee, R. T. McGibbon, R. Feldbauer, S. Lewis, S. Tygier, S. Sievert, S. Vigna, S. Peterson, S. More, T. Pudlik, T. Oshima, T. J. Pingel, T. P. Robitaille,

T. Spura, T. R. Jones, T. Cera, T. Leslie, T. Zito, T. Krauss, U. Upadhyay, Y. O. Halchenko, Y. Vázquez-Baeza, SciPy 1.0: fundamental algorithms for scientific computing in Python, Nature Methods 17 (3) (2020) 261–272.

[86] S. Kirkpatrick, C. D. Gelatt, M. P. Vecchi, Optimization by simulated annealing, Science 220 (4598) (1983) 671–680. doi:10.1126/science.220.4598.671.

[87] C. Tsallis, D. A. Stariolo, Generalized simulated annealing, Physica A: Statistical Mechanics and its Applications 233 (1-2) (1996) 395–406. doi:10.1016/S0378-4371(96)00271-3.

[88] Y. Xiang, X. G. Gong, Efficiency of generalized simulated annealing, Physical Review E 62 (3 B) (2000) 4473–4476. doi:10.1103/PhysRevE.62.4473.

[89] T. F. Anderson, D. S. Abrams, E. A. Grens, Evaluation of parameters for nonlinear thermodynamic models, AIChE Journal 24 (1) (1978) 20–29. doi:10.1002/aic.690240103.

[90] C.-Y. Gau, M. A. Stadtherr, Reliable nonlinear parameter estimation using interval analysis: Error-in-variable approach, Computers and Chemical Engineering 24 (2-7) (2000) 631–637. doi:10.1016/S0098-1354(00)00363-X.

[91] C.-Y. Gau, J. F. Brennecke, M. A. Stadtherr, Reliable nonlinear parameter estimation in VLE modeling, Fluid Phase Equilibria 168 (1) (2000) 1–18. doi:10.1016/S0378-3812(99)00332-5.

[92] I.-W. Kim, M. J. Liebman, T. F. Edgar, Robust errorinvariables estimation using nonlinear programming techniques, AIChE Journal 36 (7) (1990) 985–993. doi:10.1002/aic.690360703.

[93] R. Wittig, J. Lohmann, J. Gmehling, Vapor-liquid equilibria by UNIFAC group contribution. 6. Revision and extension, Industrial and Engineering Chemistry Research 42 (1) (2003) 183–188. doi:10.1021/ie0205061.

[94] C. Bell, Contributors, Thermo: Thermodynamics and Phase Equilibrium component of Chemical Engineering Design Library (ChEDL).

[95] D. W. Green, M. Z. Southard, Perry's Chemical Engineers' Handbook, 9th Edition, McGraw-Hill Education, New York, NY, 2019.

[96] H. Holldorff, H. Knapp, Binary vapor-liquid-liquid equilibrium of dimethyl ether - water and mutual solubilities of methyl chloride and water: Experimental results and data reduction, Fluid Phase Equilibria 44 (2) (1988) 195–209. doi:10.1016/0378-3812(88)80111-0.

[97] J. I. Partanen, L. J. Partanen, K. P. Vahteristo, Traceable Thermodynamic Quantities for Dilute Aqueous Sodium Chloride Solutions at Temperatures from (0 to 80) °C. Part 1. Activity Coefficient, Osmotic Coefficient, and the Quantities Associated with the Partial Molar Enthalpy, Journal of Chemical and Engineering Data 62 (9) (2017) 2617–2632. doi:10.1021/acs.jced.7b00091.

[98] L. J. Partanen, J. I. Partanen, Traceable Values for Activity and Osmotic Coefficients in Aqueous Sodium Chloride Solutions at Temperatures from 273.15 to 373.15 K up to the Saturated Solutions, Journal of Chemical and Engineering Data 65 (11) (2020) 5226–5239. doi:10.1021/acs.jced.0c00402.

[99] P. M. Gross, The salting out of non-electrolytes from aqueous solutions, Chemical Reviews 13 (1) (1933) 91–101. doi:10.1021/cr60044a007.

[100] L. L. Lee, A molecular theory of Setchenov's salting-out principle and applications in mixed-solvent electrolyte solutions, Fluid Phase Equilibria 131 (1-2) (1997) 67–82. doi:10.1016/s0378-3812(96)03198-6.

[101] S. Endo, A. Pfennigsdorff, K. U. Goss, Salting-out effect in aqueous NaCl solutions: Trends with size and polarity of solute molecules, Environmental Science and Technology 46 (3) (2012) 1496–1503. doi:10.1021/es203183z.

[102] M. Li, B. Zhuang, Y. Lu, L. An, Z. G. Wang, Salt-Induced Liquid-Liquid Phase Separation: Combined Experimental and Theoretical Investigation of Water-Acetonitrile-Salt Mixtures, Journal of the American Chemical Society 143 (2) (2021) 773–784. doi:10.1021/jacs.0c09420.

[103] W. F. Furter, R. A. Cook, Salt effect in distillation: A literature review, International Journal of Heat and Mass Transfer 10 (1) (1967) 23–36. doi:10.1016/0017-9310(67)90181-0.

[104] W. F. Furter, Salt effect in distillation: A literature review II, The Canadian Journal of Chemical Engineering 55 (3) (1977) 229–239. doi:10.1002/cjce.5450550301.

[105] J. M. Prausnitz, R. N. Lichtenthaler, E. G. De Azevedo, Molecular thermodynamics of fluid-phase equilibria, 3rd Edition, Prentice Hall, Upper Saddle River, NJ, 1998.

[106] R. De Santis, L. Marrelli, P. N. Muscetta, Liquid-liquid equilibria in water-aliphatic alcohol systems in the presence of sodium chloride, The Chemical Engineering Journal 11 (3) (1976) 207–214. doi:10.1016/0300-9467(76)80042-1.

[107] X. Lu, P. Han, Y. Zhang, Y. Wang, J. Shi, Salting-out separation and liquid-liquid equilibrium of Tertiary butanol aqueous solution, Chemical Engineering Journal 78 (2-3) (2000) 165–171. doi:10.1016/S1385-8947(00)00153-4.

[108] J. Hirschfelder, D. Stevenson, H. Eyring, A theory of liquid structure, The Journal of Chemical Physics 5 (11) (1937) 896–912. doi:10.1063/1.1749960.

[109] D. Hadjiev, G. Kuychoukov, A separator for liquid-liquid dispersions, The Chemical Engineering Journal 41 (2) (1989) 113–116. doi:10.1016/0300-9467(89)80078-4.

[110] S. K. Kurt, I. Vural Gürsel, V. Hessel, K. D. Nigam, N. Kockmann, Liquid-liquid extraction system with microstructured coiled flow inverter and other capillary setups for single-stage extraction applications, Chemical Engineering Journal 284 (2016) 764–777. doi:10.1016/j.cej.2015.08.099.

[111] G. M. Bollas, C. C. Chen, P. I. Barton, Refined electrolyte-NRTL model: Activity coefficient expressions for application to multi-electrolyte systems, AIChE Journal 54 (6) (2008) 1608–1624. doi:10.1002/aic.11485.

[112] Y. Hao, C.-C. Chen, Nonrandom Two-Liquid Segment Activity Coefficient Model with Association Theory, Industrial & Engineering Chemistry Research 58 (28) (2019) 12773–12786. doi:10.1021/acs.iecr.9b02078.

[113] Y. Hao, C. Chen, Nonrandom two-liquid activity coefficient model with association theory, AIChE Journal (e17061) (2020) 1–12. doi:10.1002/aic.17061.

[114] C. C. Chen, P. M. Mathias, H. Orbey, Use of hydration and dissociation chemistries with the electrolyte-NRTL model, AIChE Journal 45 (7) (1999) 1576–1586. doi:10.1002/aic.690450719.